FUSION ENERGY DIVISION LIBRARY
OCT 17 1980
OAK RIDGE NATIONAL LABORATORY LIBRARIES
3 4456 0539375 8

ORNL/SUB-33200/3

Cy. 23

HUGHES
HUGHES AIRCRAFT COMPANY
ELECTRON DYNAMICS DIVISION

DEVELOPMENT PROGRAM FOR A 200 kW, CW GYROTRON

K. W. Arnold, J. J. Tancredi, M. Caplan, K. W. Ha,
D. N. Birnbaum, W. Weiss

QUARTERLY REPORT NO. 3
JANUARY THROUGH MARCH 1980

Contract No. W-7405-ENG-26

Prepared by

HUGHES AIRCRAFT COMPANY
Electron Dynamics Division
3100 West Lomita Boulevard
Torrance, California 90509

for
OAK RIDGE NATIONAL LABORATORY
Oak Ridge, Tennessee 37830
operated by
UNION CARBIDE CORPORATION
for the
DEPARTMENT OF ENERGY

This report was prepared as an account of work sponsored by an agency of the United States Government. Neither the United States Government nor any agency thereof, nor any of their employees, contractors, subcontractors, or their employees, makes any warranty, express or implied, nor assumes any legal liability or responsibility for any third party's use or the results of such use of any information, apparatus, product or process disclosed in this report, nor represents that its use by such third party would not infringe privately owned rights.

ORNL/SUB–33200/3

HUGHES

HUGHES AIRCRAFT COMPANY

ELECTRON DYNAMICS DIVISION

DEVELOPMENT PROGRAM FOR A 200 kW, CW GYROTRON

K. W. Arnold, J. J. Tancredi, M. Caplan, K. W. Ha,
D. N. Birnbaum, W. Weiss

QUARTERLY REPORT NO. 3
JANUARY THROUGH MARCH 1980

Contract No. W-7405-ENG-26

Prepared by

HUGHES AIRCRAFT COMPANY
Electron Dynamics Division
3100 West Lomita Boulevard
Torrance, California 90509

for
OAK RIDGE NATIONAL LABORATORY
Oak Ridge, Tennessee 37830
operated by
UNION CARBIDE CORPORATION
for the
DEPARTMENT OF ENERGY

TABLE OF CONTENTS

Section		Page
I.	INTRODUCTION	1-1
II.	PROGRESS	2-1
	2.1 General	2-1
	2.2 Magnetron Injection Gun	2-1
	2.3 RF Cavity Design	2-3
	2.4 Power Supply	2-4
III.	SCHEDULE	3-1
IV.	REFERENCES	4-1
Appendix		
A	DESIGN AND ANALYSIS OF GYROTRON OSCILLATOR CAVITIES	A-1

LIST OF ILLUSTRATIONS

Figure		Page
1-1	Schematic of gyrohron oscillator showing applied magnetic field and the rf field and gain in the cavity.	1-3
2.2-1	Magnetron injection gun for 60 GHz gyrotron.	2-2

I. INTRODUCTION

The objective of this program is the design and development of a millimeter-wave device to produce 200 kW of continuous-wave power at 60 GHz. The device, which will be a gyrotron oscillator, will be compatible with power delivery to an electron-cyclotron plasma. Smooth control of rf power output over a 17 dB range is required, and the device should be capable of operation into a severe time-varying rf load mismatch.

The technical baseline for the gyrotron and the associated power supply are shown in Table I. In the gyrotron, which is shown schematically in Figure 1-1, the electrons are formed into a hollow beam by a magnetron-injection electron gun with a considerable amount of their energy in rotation. A gradually rising magnetic field compresses the beam in diameter and at the same time increases the orbital energy according to the theory of adiabatic invariants until approximately 2/3 of the beam energy is in rotation and the rotational frequency is 60 GHz; at this point the magnetic field becomes uniform and the beam enters a quasi-optical open cavity where the spinning electrons interact with the eigen mode of the cavity. The rf energy builds up at the expense of the rotational energy of the dc beam. The spent beam enters the region of decreasing magnetic field, undergoes decompression and impinges on the collector. The latter also functions as the output waveguide. In order to handle the power in the spent beam and the power dissipation in the window the output waveguide tapers up from the cavity diameter to an appropriate value.

The duration of the program is 36 months, to encompass the building and test of up to twelve devices. The magnetron injection gun is well understood and allows the user of the extraction anode (as well as cathode temperature variation) to vary the rf power out. At least two design approaches will be taken with respect to the collector, which has to be able to dissipate over 560 kW in undepressed operation. Fabrication and processing of prototype devices will proceed in parallel.

TABLE I

The Gyrotron	
Frequency	60 GHz
Power out	200 kW RF
Electronic efficiency	35%
Beam voltage	70 kV
Beam current	8.0 A
Magnetic field	23.0 kG
Transverse to longitudinal velocity ratio	1.5
Cathode Loading	4.5 A/cm^2
Cathode radius	0.60 cm

The Power Supply	
Voltage rating	100 kV dc
Current rating	10 A
Anode supply voltage	0-35 kV dc
Anode supply current	<20 mA
Heater supply voltage	0-15 V, ac
Heater supply current	15 A
Operating Modes:	
1.	10 μs pulse length
2.	1 ms - 100 ms pulse length
3.	30 s to cw

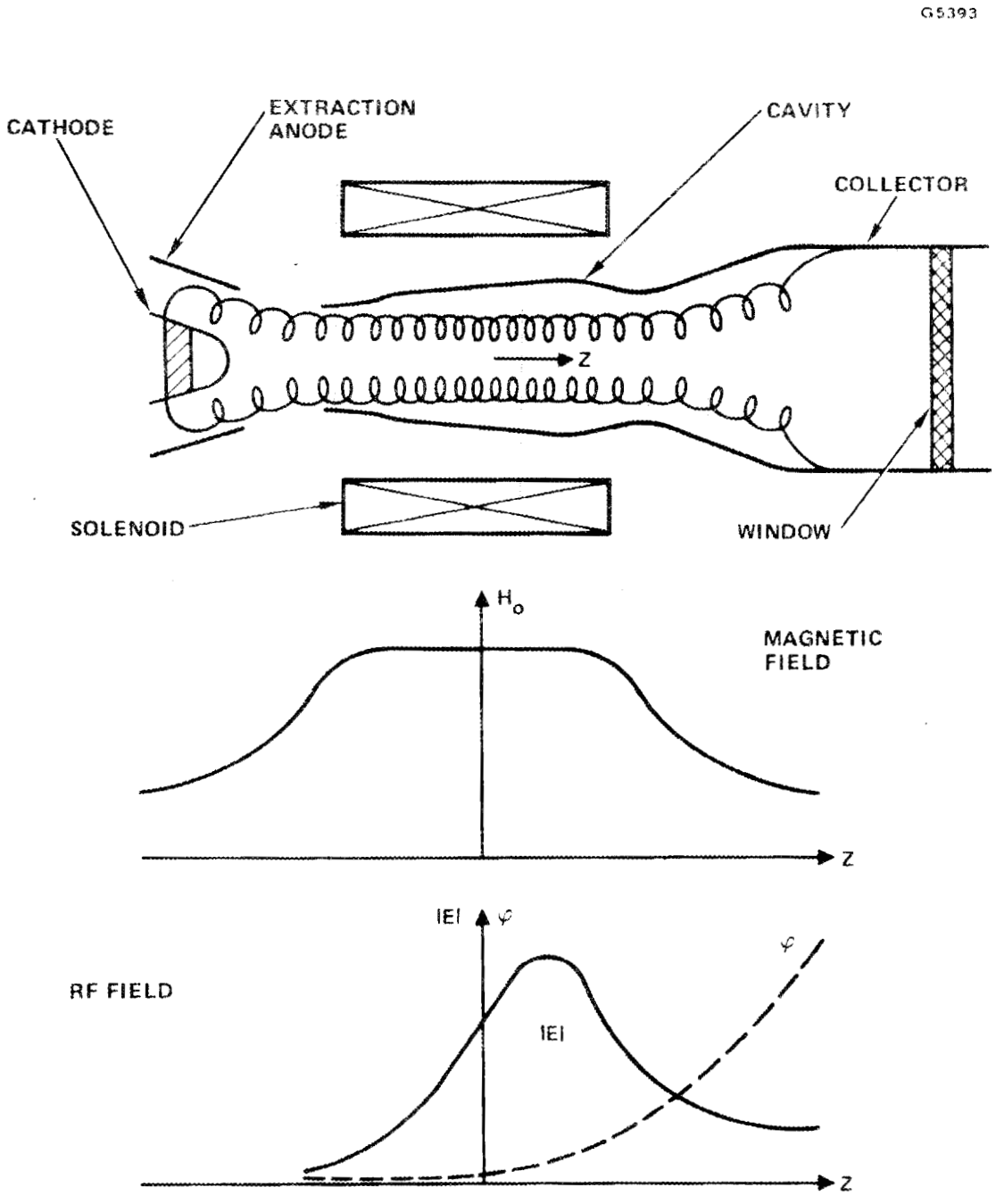

Figure 1-1 Schematic of gyrohron oscillator showing applied magnetic field and the rf field and gain in the cavity.

II. PROGRESS

2.1 GENERAL

Effort for this report period has been concentrated in the following tasks:

- Magnetron Injection Gun
- RF Circuit
- Power Supply

2.2 MAGNETRON INJECTION GUN

The magnetron injection gun was designed and finalized during this report period. A computer trajectory plot of the gun and acceleration region is shown in Figure 2.2-1. Salient characteristics of the gun are tabulated in Table 2.2-1.

This gun design is a further extrapolation of the modified gun design achieved for 110 GHz gyrotrons.[1] The anode voltage provides a sensitive control of the amount of beam energy which is converted to transverse energy. This value is selected to convert 67% of the beam energy to the transverse energy. Depending on the amount of transverse velocity spread in the beam, more energy could be converted to the transverse direction to be used for interaction.

The transverse velocity spread due to space charge and geometrical effects of the gun shown in Figure 2.2-1 is predicted to be 1.7%, assuming the beam is adiabatically invariant. If this attractively low spread can actually be achieved, even more than 67% of the beam energy could be transformed to the transverse direction.

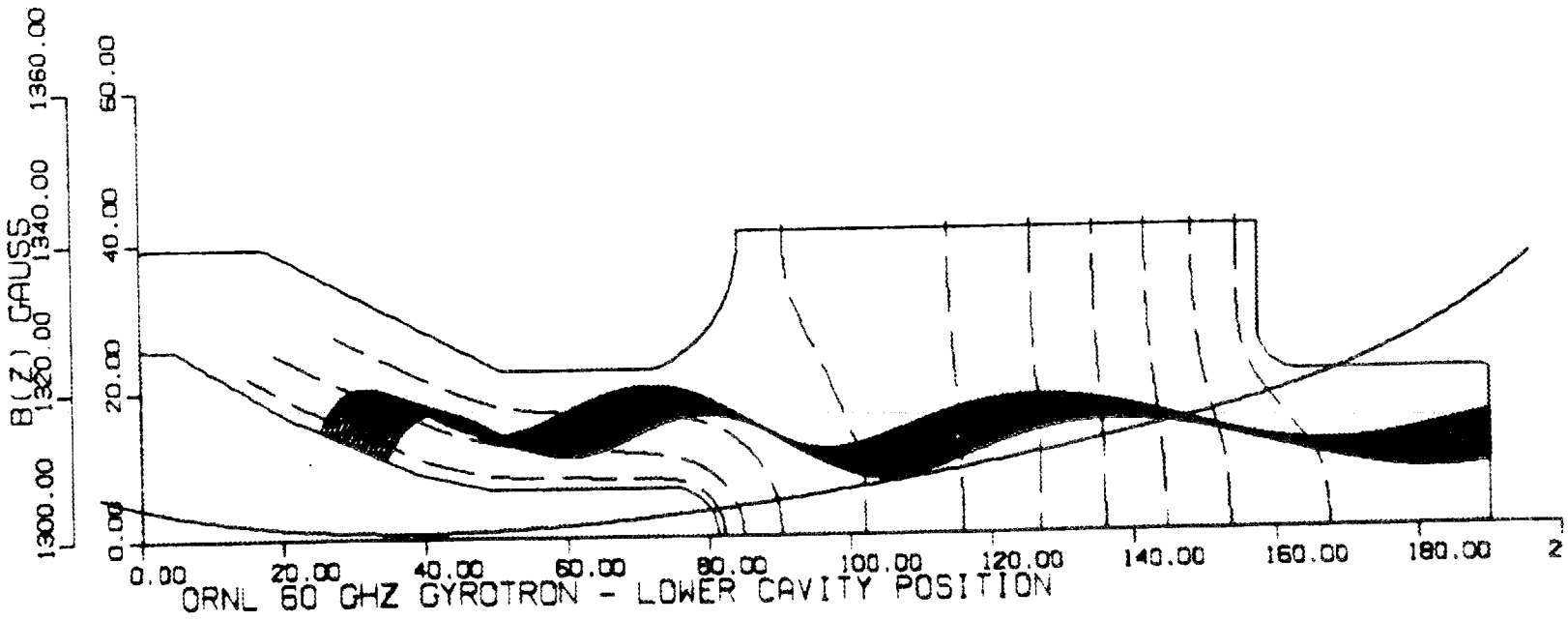

Figure 2.2-1 Magnetron injection gun for 60 GHz gyrotron.

TABLE 2.2-1

Cathode Current Density	4.0 A/cm^2 (7 amps)
Cathode Radius	0.6 cm
Ra/Rc	2.46
I_{TL}/I_{SC}	17%
B_c	1300 gauss
Anode Voltage	23 kV

The exact shape of the magnetic field required in the region between the gun and cavity directly affects the adiabatic invariance of the beam. The required shape has not yet been determined, although it appears that the cavity must be located approximately 25-30 cm from this cathode nose.

A superconducting solenoid containing eight separate coils is being investigated to determine the necessary field shape required. Eight coils provide sufficient flexibility in field shaping and will also provide tapering of the field over the cavity for efficiency enhancement. In a final solenoid design, the number of active coils can be reduced to three.

2.3 RF CAVITY DESIGN

The existing Hughes cavity codes have been modified to provide calculations of Q for tapered cavities. This effort has been incorporated into Hughes Technical Report No. 58, which is included as an Appendix to this report.

Based on this new design tool, a computer analysis of several attractive cavities will be undertaken. In order to verify these computer results, cold tests cavities will be fabricated and measured at X-band.

2.4 POWER SUPPLY

As reported in the last report, the MSR high voltage power supply at the Kwajalein Missile Range has been excessed by the Army. A Hughes EDD representative and a representative from an international moving company were sent to Kwajalein to evaluate the condition of the equipment and to provide an estimate for moving the power supply.

The power supply was found to be in reasonably good condition. Of the existing transmitter equipment, the entire high voltage power supply is usable, including the 4160V reactors, ignitron pre-regulators, and circuit breaker cabinets. It was also determined that a major portion of the water cooling system would be available, as well as interconnecting cable, busses, duct work and a motor control center. The MSR modulator was determined to be pulse width limited and not realistically usable without extensive modification.

The disassembly of equipment should be undertaken in a logical and orderly fashion by competent personnel who will be available to reassemble it at a later date, and in an efficient manner. Arrangements were therefore made to have personnel from Hughes Ground Systems Group perform the disassembly and reassembly. It was estimated that two man-months would be required for disassembly.

The move of MSR equipment to Hughes EDD was estimated to require 17 shipping containers.

III. SCHEDULE

The program schedule and current status is attached.

MILESTONE SCHEDULE AND STATUS REPORT — 60 GHz 200 KW GYROTRONS

HUGHES EDD, TORRANCE, CA 90509 | REPORTING PERIOD 3/80 | CONTRACT NO. | FOR UNION CARBIDE CO., OAK RIDGE, TN. | SHEET 1 OF 1

TASK NO.	TASK TITLE
-1100	MAGNETRON INJECTION GUN DESIGN
-1200	DIODE GUN DESIGN
-1300	SOLENOID DESIGN
-1400	RF CIRCUIT DESIGN
-1510	COLLECTOR 1.
-1520	COUPLER 1.
-1610	COLLECTOR 2.
-1620	COUPLER 2.
-1900	INTERFACE/LAYOUT
-2110	BEAM
-2120	BEAM ANALYZER FABRICATE
-2130	BEAM ANALYZER TEST
-2210	BEAM TESTER/ANALYZER DESIGN
-2220	FABRICATE
-2230	FOCUS TESTS
-2240	THERMAL TESTS
-3110	FABRICATE SN/1
-3120	TEST SN/1
-3210	FABRICATE SN/2
-3220	TEST SN/2
-3310	FABRICATE SN/3
-3320	TEST SN/3
-5100	POWER SUPPLY
-5200	RF TEST EQUIPT
-6000	REPORTS MONTHLY
	QUARTERLY

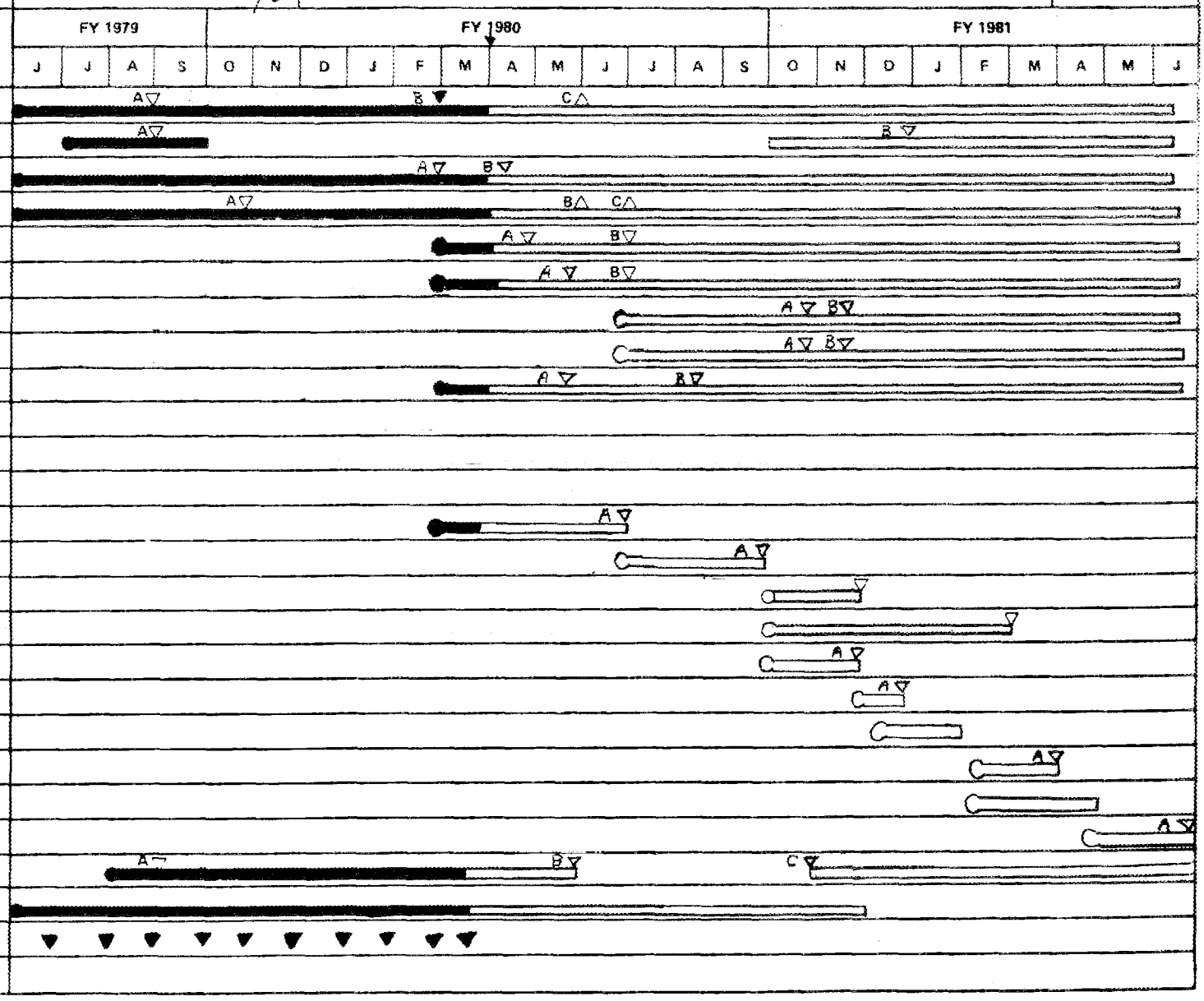

IV. REFERENCES

1. Arnold, KW, et al, Development Program for a 200 kW, CW, 110 GHz Gyrotron, Quarterly Report No. 1, prepared by Hughes Aircraft Company for Oak Ridge National Laboratory under Contract No. W-7405-ENG-26, ORNL/SUB-33200/1, June through September 1979.

APPENDIX A

DESIGN AND ANALYSIS OF GYROTRON OSCILLATOR CAVITIES

W-08476

TECHNICAL REPORT NUMBER 58
DESIGN AND ANALYSIS OF GYROTRON OSCILLATOR CAVITIES

BY

MALCOLM CAPLAN

MARCH 1980

HUGHES AIRCRAFT COMPANY
ELECTRON DYNAMICS DIVISION
3100 WEST LOMITA BOULEVARD
TORRANCE, CALIFORNIA 90509

TABLE OF CONTENTS

Section		Page
I.	INTRODUCTION	1
II.	THEORETICAL EVALUATION OF THE MODE STRUCTURE, RESONANT FREQUENCY AND Q FACTORS FOR AN ARBITRARY SHAPED CYLINDRICAL SYMMETRIC CAVITY	4
III.	EXPERIMENTAL DETERMINATION OF CAVITY Q RESONANT FREQUENCY AND MODE STRUCTURE	20
IV.	DETERMINATION OF CAVITY OUTPUT POWER AND EFFICIENCY	27
V.	RF POWER DISSIPATION	38
VI.	CONCLUSIONS AND FUTURE STUDY	40

I. INTRODUCTION

In the discussion that follows, it is assumed that the first phase of gyrotron design has been completed; a desired transverse mode has been chosen and an electron beam of known voltage, current, perpendicular energy and beam position has been designed. One wishes to optimize the RF power that can be extracted from such a beam through appropriate cavity design; cavity design referring to both the design of the metal structure as well as the external magnetic profile contained within. Although optimum efficiency is the primary goal, the final design must be compatible with the following constraints:

- RF loading on cavity walls must be kept below the level at which it would be impossible to cool the surface adequately (roughly 1000 watts/sqcm).

- The cavity should be adequately isolated from the outside world so that loading effects far from the cavity will not greatly affect gyrotron operation.

- The cavity operation should exhibit mode selectivity and stability. The start threshold currents for the desired mode should be lower than those for other nearby modes and there should be adequate mode separation to prevent unwanted modes from being excited.

The procedure for design is to first determine theoretically and/or experimentally the "cold test" properties of a given cavity namely:

1. external Q
2. unloaded Q
3. mode structure and frequency

This information is then used as input for the numerical simulation of the electron beam interacting with the cavity fields. The results of these computer simulations are then combined self-consistently with the "cold test" information to give the RF efficiency of the cavity and the resulting wall loading. This analysis is repeated for a variety of design choices until a prefered design is found.

The parameters which will characterize a cavity design are:

• maximum cavity radius	a
• effective cavity length	L
• ratio of cyclotron frequency to doppler shifted operating frequency	XFACT
• percent taper of axial magnetic field	DELTB
• taper angle of main cavity wall	THETA
• external cavity Q	Q_{EXT}
• unloaded cavity Q	Q_{WALL}
• loss constant defined as the power leaking through the cavity hole for a normalized field amplitude of one.	KLOSS

All illustrative cavity designs given are for operation in the TE_{021} mode and assume the following beam parameters:

Voltage ---------- 80 kv

Current ---------- 2 - 8 amps

Beam Position ---- 1st maximum of TE_{021} mode

Rotational energy ---- 70% of total energy.

II. THEORETICAL EVALUATION OF THE MODE STRUCTURE, RESONANT FREQUENCY AND Q FACTORS FOR AN ARBITRARY SHAPED CYLINDRICAL SYMMETRIC CAVITY

It is useful to make some rough estimates for the resonant frequency and external Q of a cavity.

RESONANT FREQUENCY

The resonant frequencies for TE modes in an ideal closed cylindrical cavity are given by:

$$\omega_{mn\ell} = \frac{c}{a}\sqrt{k_{mn}^2 + \left(\frac{\ell\pi a}{L}\right)^2} \qquad (1)$$

where

m	is azimuthal mode number
n	is radial mode number
ℓ	is longitudinal mode number
k_{mn}	is the nth root of the derivative of the mth order bessel function
m,n,ℓ	are integers, a is the cavity radius and L is the cavity length.

EXTERNAL Q

One begins with the basic definition for Q_{EXT}.

$$Q_{EXT} = \frac{\text{(angular frequency) x (stored cavity energy)}}{\text{(power out)}}$$

Stored cavity energy = $L\bar{A}\varepsilon$ where:

L = cavity length

$\bar{A}$ = average cross sectional area

ε = average energy density

Power out = $(1 - R)\, V_g\, A\varepsilon$ where:

A = effective area of opening

R = reflection coefficient for wave propagating towards output

V_g = group velocity of wave propagating toward output.
$V_g = c^2 \ell^2 \pi / L\omega_{mn\ell}$

Substituting and making the approximation $\omega_{mn\ell} \approx \frac{ckmn}{a}$ one obtains:

$$Q_{EXT} = \frac{k_{mn}^2 \, (L/a)^2}{(1 - R)\pi\ell^2} \left(\frac{\bar{A}}{A}\right) \tag{2}$$

For cavities of constant cross section ($A = \bar{A}$), the minimum Q occurs when $R = 0$ and $\ell = 1$, giving the following definition for Q_{min}:

$$Q_{min} = \frac{k_{mn}^2 \, (L/a)^2}{\pi} \tag{3}$$

The actual Q_{EXT} and resonant frequency of any arbitrary shaped cavity will be written as:

$$\omega_{mn\ell} = \frac{c}{a}\sqrt{k_{mn}^2 + \left(\frac{\ell_{EF}\ \pi a}{L}\right)^2} \tag{4a}$$

$$Q_{EXT} = Q_F \times Q_{min} = Q_F \times \frac{(L/a)^2\ k_{mn}^2}{\pi} \tag{4b}$$

where

Q_F is a correction factor expressing the ratio of the true Q_{EXT} to Q_{min}

ℓ_{EF} is the effective longitudinal mode number whose true value will differ from the integer values for an ideal cavity

a is the maximum cavity radius.

The basic assumption in these definitions is that the <u>transverse</u> mode structure can be described by bessel functions even for cavities whose dimensions vary in the longitudinal direction.

EIGENVALUE EQUATION FOR DETERMINATION OF FIELD STRUCTURE, Q_{EXT} and $\omega_{mn\ell}$ ($TE_{mn\ell}$ modes)

An expression for the transverse electric field amplitude in an arbitrary profiled cavity can be written as:

$$E_\theta = \text{Real}\left\{E_o \cdot E(z)\ J_m'\ [k_{mn}\ r/a(z)]\ \cos m\theta e^{i\omega t}\right\} \tag{5}$$

where:

$a(z)$ gives the cavity radius as a function of axial position z

ω is the complex frequency $= \omega_R + i\omega_I$

$E(z)$ is the complex field profile as a function of z.
$E(z) = |E(z)|\ e^{i\phi(z)}$

E_o is the maximum field amplitude

J_m is the bessel function of order m

Q_{EXT} can be related to ω_I since:

$$Q_{EXT} = \frac{\omega_R \cdot \text{stored cavity energy}}{\text{power out}}$$

$$\text{power out} = \frac{d}{dt}\,(\text{cavity energy}) = 2\omega_I\,(\text{cavity energy})$$

$$Q_{EXT} = \frac{\omega_R}{2\omega_I} \tag{5}$$

For an ideal closed cavity $Q_{EXT} \to \infty$, $\omega_I \to 0$ and $E(z) \to \sin(\ell\pi z/L)$.

By substituting expression (5) for E_θ into Maxwell's equations, one obtains to lowest order the following complex eigenvalue differential equation:

$$\boxed{\frac{d^2E(z)}{dz^2} + \left[\omega^2 - \frac{k_{mn}^2}{a^2(z)}\right] E(z) = 0} \tag{7}$$

Solutions of this equation which satisfy the proper boundary conditions will give the axial mode structure, the resonant frequencies (ω_R) and Q_{EXT} ($\omega_R/2\omega_I$).

The boundary conditions to be satisfied at each end of the cavity are:

Right hand side of cavity ($z = z_2$)

Outgoing travelling wave to the right

$E(z) \alpha \exp(-ih_2 z)$ or $\frac{dE}{dz} + ih_2 E(z) = 0$ at $z = z_2$

Left hand side of cavity ($z = z_1$)

exponentially decaying wave to the left in the below cutoff region.

$E(z) \alpha \exp(ih_1 z)$ or $\frac{dE}{dz} - ih_1 E(z) = 0$ at $z = z_1$

where

$$h_2 = \sqrt{\omega^2 - \frac{k_{mn}^2}{a^2(z_2)}}$$

$$h_1 = -i\sqrt{\frac{k_{mn}^2}{a^2(z_1)} - \omega^2}$$

NUMERICAL SOLUTION

The differential equation is cast into a form convenient for solution, using the following definitions:

E_1 = real $E(z)$

E_2 = d/dz [real $E(z)$]

E_3 = imaginary $E(z)$

E_4 = d/dz [imaginary $E(z)$]

a = maximum cavity radius

$R(z)$ = cavity profile vs z normalized by a

Q = Q_{EXT}

$\bar{\omega}_R^{\,2} = (k_{mn}^2 + \delta^2)/(1 - 1/4Q^2)$

$\omega_R = c\bar{\omega}_{R/a}$ = resonant frequency

$$\delta \approx \frac{\pi\, \ell_{EF}}{L}$$

$$dE_1/dz = E_2$$

$$dE_2/dz = h_R^2 E_1 + h_I^2 E_3$$

$$dE_3/dz = E_4$$

$$dE_4/dz = -h_R^2 E_3 - h_I^2 E_4$$

$$h_R^2(z) = \delta^2 + k_{mn}^2 \left[1. - \frac{1.}{R(z)^2}\right]$$

$$h_I^2 = \frac{k_{mn}^2 + \delta^2}{Q(1 - 1/4\, Q^2)}$$

at $z = z_1$

$$E_1 = 1$$

$$E_2 = \sqrt{\frac{(h_R^2 + h_I^2)^{1/2} + |h_R|}{2}}$$

$$E_3 = 0$$

$$E_4 = -\sqrt{\frac{(h_R^2 + h_I^2)^{1/2} - |h_R|}{2}}$$

at $z = z_2$

$$|m|^2 = |(E_2 - h_R E_3 - h_I E_1)^2 + (E_4 + h_R E_1 - h_I E_3)^2| \equiv 0$$

In order to solve the boundary condition at $z = z_2$, a systematic searching procedure is used to find δ and Q which will make $|m| = 0$. Figure 1 shows the initial grid which is set up to span the range where the actual values of Q and δ may lie. For each value of Q and δ in the grid, the differential system is solved, $|m|$ is then found and a new smaller grid system is set up surrounding the value of δ and Q which led to minimum $|m|$. The process is repeated until sufficiently accurate values for δ and Q are found which make $|m| \to 0$ to the desired accuracy.

FINAL FIELD EQUATIONS

When the longitudinal mode structure equation has been solved, the complete electromagnetic field can be specified along with Q_{EXT} and the resonant frequency. For $TE_{on\ell}$ modes these are given as

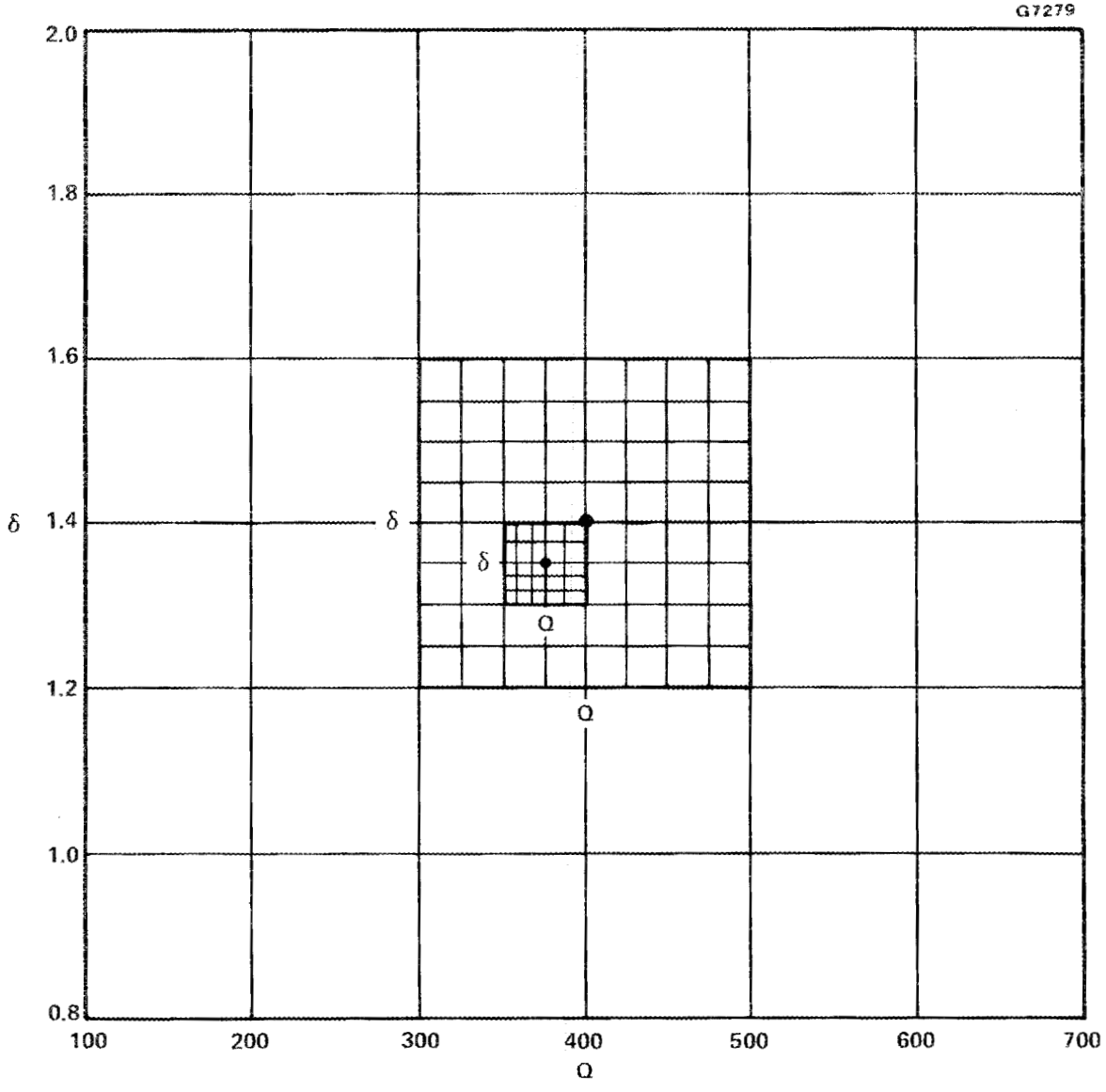

Figure 1 Grid search for δ and Q.

$$E_\theta = E_o J_1\left(\frac{k_{mn} r}{R(z)}\right) [E_R(z) \cos(\omega t) - E_I(z) \sin(\omega t)] \tag{8a}$$

$$B_R = \frac{E_o}{\omega/c} J_1\left(\frac{k_{mn} r}{R(z)}\right) \left[\frac{dE_R(z)}{dz} \sin(\omega t) + \frac{dE_I(z)}{dz} \cos(\omega t)\right] \tag{8b}$$

$$B_z = \frac{-k_{mn}}{\omega/c} E_o J_o\left(\frac{k_{mn} r}{R(z)}\right) [E_R(z) \sin(\omega t) + E_I(z) \cos(\omega t)] \tag{8c}$$

where

E_θ = transverse electric field

B_R = radial RF magnetic field

B_z = longitudinal RF magnetic field

$E_R(z) = E_1(z)$ = real part $E(z)$

$E_I(z) = E_3(z)$ = imaginary part of $E(z)$

ω = resonant frequency $= \frac{c}{a}\sqrt{k_{mn}^2 + \frac{\ell_{EF}^2 \pi^2}{(L/a)^2}}$

$\ell_{EF} = \sqrt{\frac{1 + k_{mn}^2/4Q^2\delta^2}{1 - 1/4Q^2}} \left(\frac{\delta L}{\pi}\right)$ = effective longitudinal mode no.

POWER LOSS CONSTANT

A power loss constant kLOSS can be calculated from the known value of Q_{EXT} and the field structure which relates the power drained from the cavity opening to the square of the peak normalized electric field.

Power loss is defined by:

$$\text{power loss} = \frac{\omega \cdot (\text{cavity energy})}{Q_{EXT}}$$

or

$$\text{power loss} = \frac{\omega}{Q_{EXT}} \int \frac{(E_\theta^2 + B_R^2 + B_z^2)}{8\pi} \, d^3V = \text{KLOSS} \cdot \bar{E}_\theta^2$$

where

$$\bar{E}_\theta = \frac{E_o ea}{mc^2}$$

Substituting the field equations and averaging over time, one obtains the following expression for KLOSS:

$$\text{KLOSS} = \frac{J_o^2 (k_{mn}) \, \bar{\omega}_R (L/a)}{16 \, Q_{EXT}}$$

$$\cdot \left[1 + \frac{k_{mn}^2}{\bar{\omega}_R^2 L} \int_o^L |E|^2 \, dz + \frac{1}{\bar{\omega}_R^2 L} \int_o^L \left|\frac{dE}{dz}\right|^2 dz \right] \qquad (9)$$

It is necessary to know KLOSS for self-consistently evaluating cavity efficiency.

UNLOADED Q AND WALL POWER DISSIPATION

The unloaded Q is determined by the wall conductivity and frequency. For a straight cavity it is given by (for $TE_{on\ell}$ modes):

$$Q_{wall} = \frac{9480.4 \sqrt{\frac{\alpha}{f}} \left[k_{mn}^2 + \left(\frac{\ell \pi a}{L} \right)^2 \right]^{3/2}}{\left[k_{mn}^2 + \left(\frac{2 \ell \pi a}{L} \right)^2 \frac{a}{L} \right]} \tag{10}$$

where

f = frequency in GHz

α = relative conductivity = 5.8 for copper.

Since $(\ell \pi a/L)$ is usually much less than k_{mn}, the expression for Q_{wall} becomes:

$$Q_{wall} = \frac{22832 \cdot k_{mn}}{\sqrt{f}} \tag{11}$$

The fraction of RF power leaving the cavity which is absorbed by the walls can be calculated from a knowledge of Q_{EXT} and Q_{wall}.

$$Q_{EXT} = \frac{\omega \text{ energy}}{\text{power out}}$$

$$Q_{wall} = \frac{\omega \text{ energy}}{\text{power walls}}$$

$$\frac{\text{power walls}}{\text{power out}} = \frac{Q_{EXT}}{Q_{wall}} \tag{12}$$

Thus once the output power has been determined, the power dissipation in the walls can be found from Equation (12). It should be noted that in all cases of interest $Q_{wall} >> Q_{EXT}$ and, hence, the total cavity Q is essentially given by Q_{EXT}.

CAVITY TAPERING

The above procedure was applied to a variety of cavities with different wall tapers. Figures 2, 3, and 4 show cavities with field tapers of 0°, 0.485° and 7°, respectively. It is to be noted that as the taper angle increases, the external Q decreases and the mode becomes more sharply peaked, the peak amplitude moving toward the cavity opening. For large taper angles, Q_{EXT} becomes less than Q_{min}. This can be understood from the approximate expression for Q_{EXT}:

$$Q_{EXT} \approx \frac{k_{mn}^2 \ (L/a)^2}{(1 - R)\ \pi} \cdot \frac{\bar{A}}{A} = \frac{Q_{min}}{1 - R} \cdot \frac{\bar{A}}{A}$$

In a strongly tapered cavity the average cross section $\bar{A}$ can become much less than the output cross section allowing Q_{EXT} to be less than Q min. Figure 5 shows a plot of Q_{EXT} versus taper angle and shows that Q_{EXT} rapidly decreases as the taper angle is increased from 0° to 1°. One may note that for the TE_{021} mode at 60 GHz, Q_{EXT} is roughly 1 - 5% of the unloaded wall loss Q.

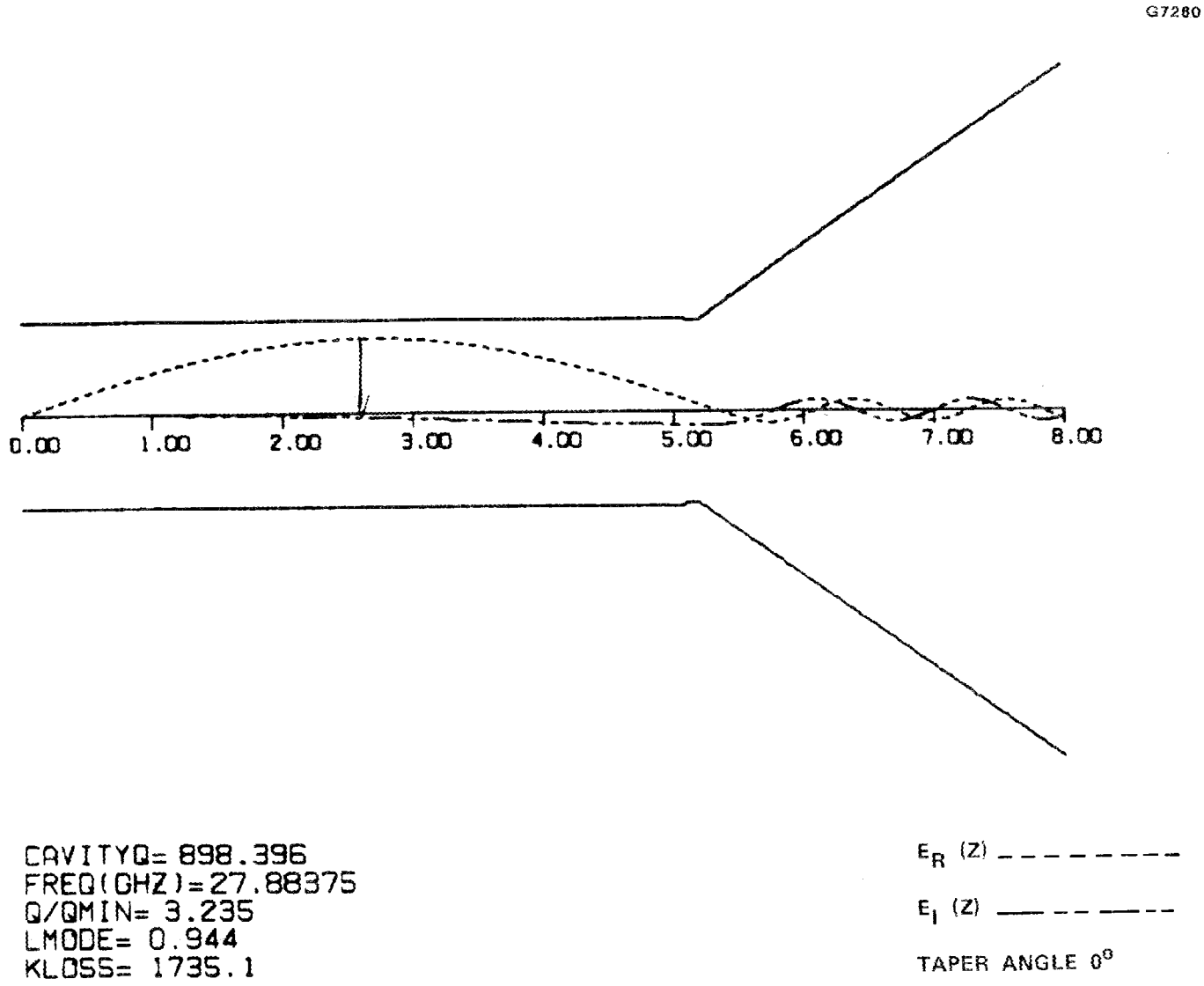

Figure 2 Computer cavity cold test.

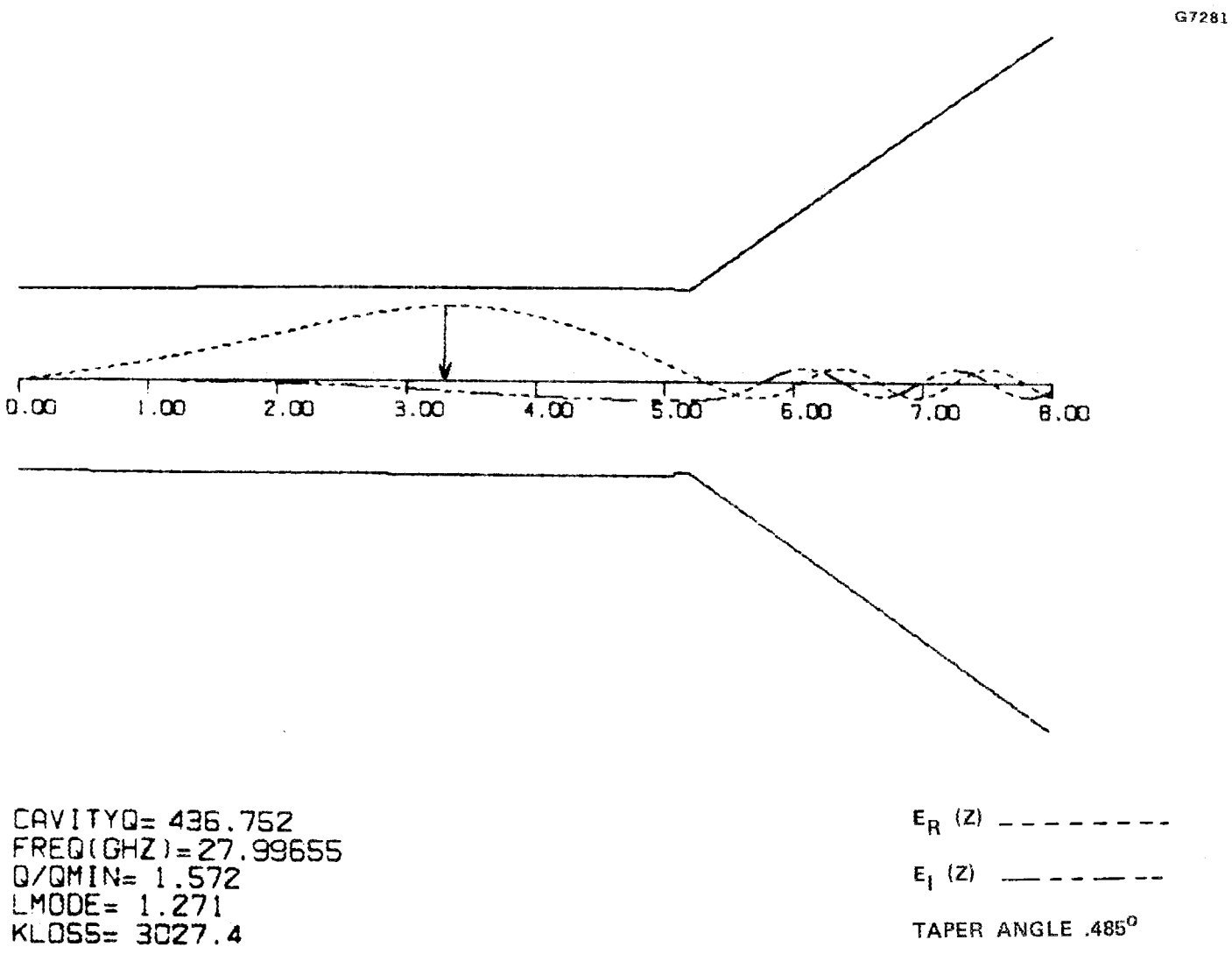

Figure 3 Computer cavity cold test.

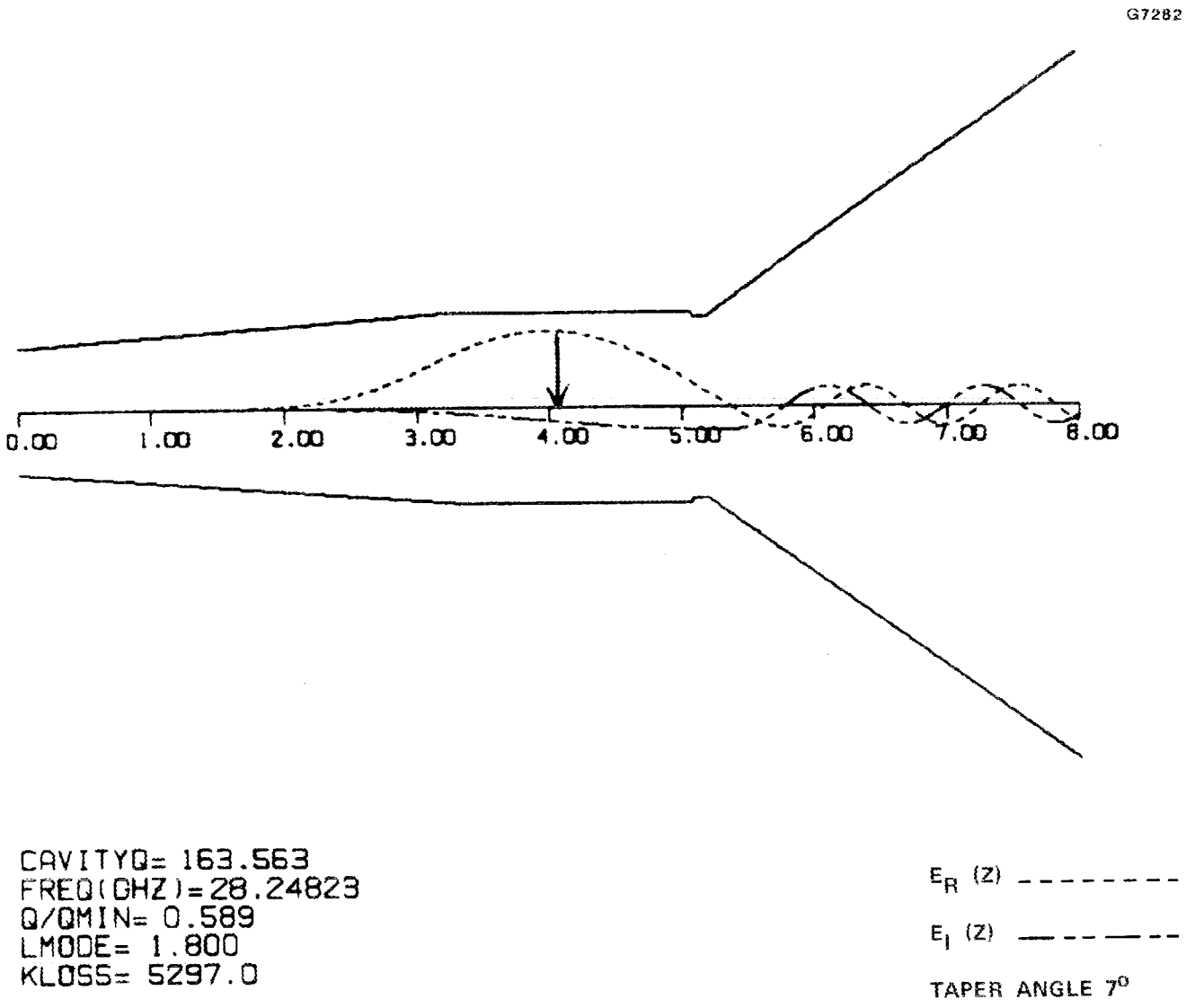

Figure 4 Computer cavity cold test.

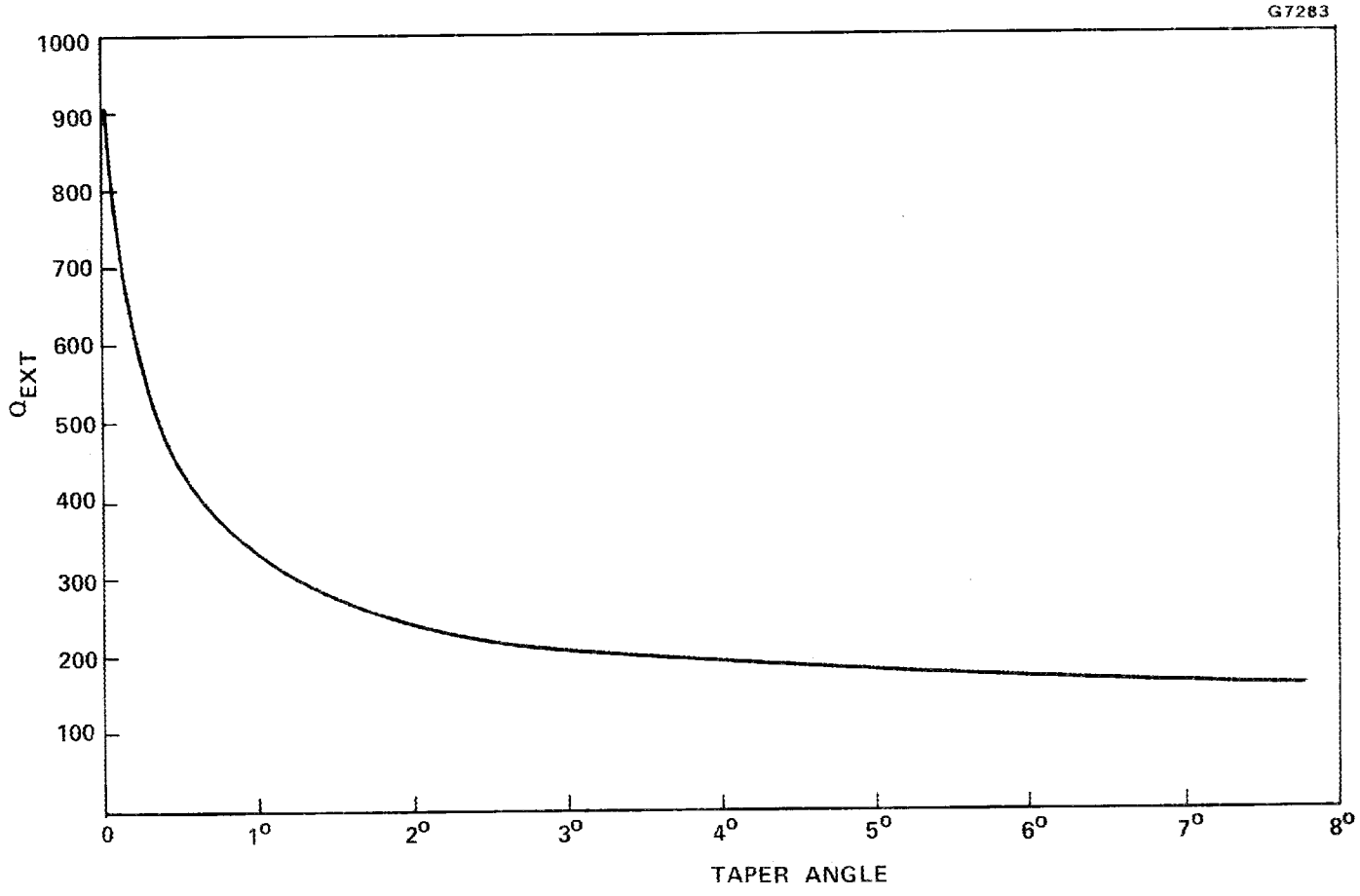

Figure 5 External Q vs taper angle.

III. EXPERIMENTAL DETERMINATION OF CAVITY Q, RESONANT FREQUENCY AND MODE STRUCTURE

The cavity Q can be determined by measuring the effective input impedance to the cavity versus frequency. An electric circuit analog of an RF source coupled into a cavity through a coupling port is shown in Figure 6a. The equivalent transformed circuit is shown in Figure 6b. The normalized input impedance at a - a is given as:

$$\frac{Z_{aa}}{Z} = i\left(\frac{\omega L}{Z}\right) + \frac{\beta}{1 + 2iQ_o\delta} \tag{13}$$

where

$Q_o = \omega L_c/R_c$ = total cavity Q without coupling port

$\beta = (\omega M)^2/ZR_c$ = coupling coefficient of external coupling port to cavity

$\delta = (\omega - \omega_o)/\omega_o$ = fractional deviation from resonance frequency ω_o

$$\omega_o = 1/\sqrt{L_c C}$$

The external Q_{EXT} due to the coupling port alone is defined as:

$$Q_{EXT} = Q_o/\beta$$

The total loaded Q_L is defined as:

$$Q_L = Q_o/(1 + \beta)$$

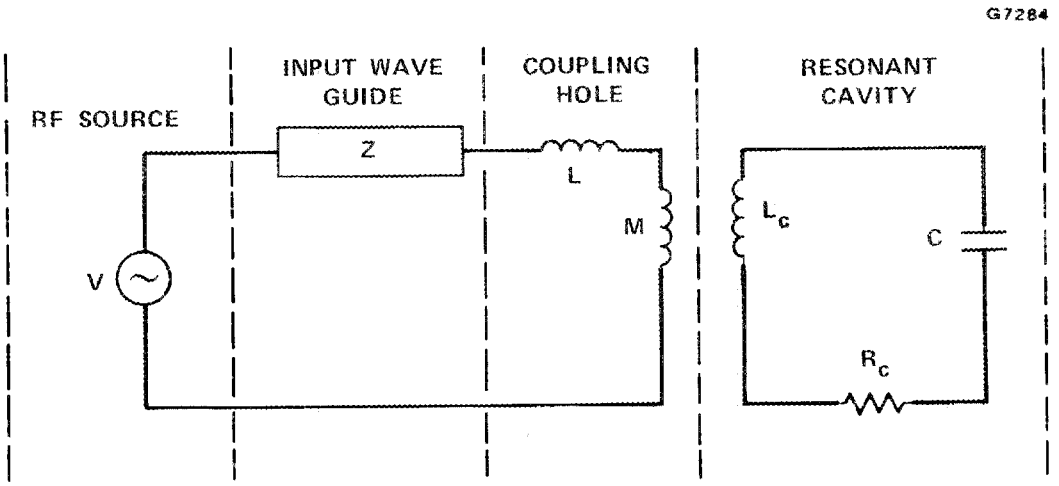

Figure 6a Equivalent circuit of RF coupled into resonant cavity.

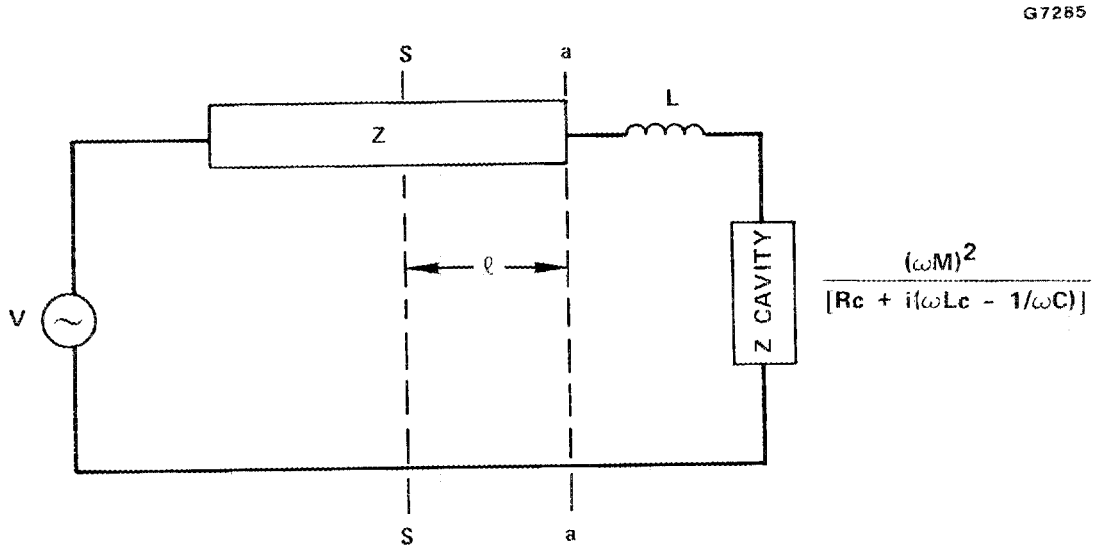

Figure 6b Equivalent representation of above circuit.

The impedance can be transformed to the detuned short position s - s by moving a distance ℓ where:

$$\ell = (-1/\beta) \cdot \tan^{-1} (\omega L/Z)$$

The normalized impedance at s - s is approximately given by:

$$Z_{ss}/Z = \frac{\beta}{1 + 2iQ_o\delta} \tag{14}$$

One observes the following properties of Z_{ss}/Z

i) $Z_{ss}/Z = \beta$ when $\delta = 0$

ii) $Z_{ss}/Z = \beta/(1 \pm i)$ when $2Q_o\delta = \pm 1$

iii) $Z_{ss}/Z = \beta/[1 \pm i(1 + \beta)]$ when $2Q_L\delta = \pm 1$

iv) $Z_{ss}/Z = \beta/(1 \pm i\beta)$ when $2Q_{EXT}\delta = \pm 1$

Using the definitions:

R = real (Z_{ss}/Z)

X = imaginary (Z_{ss}/Z)

G = real (Z/Z_{ss})

Y = imaginary (Z/Z_{ss})

one obtains:

$$Q_L = \frac{f_o}{f_1 - f_2} \quad \text{where } f_1, f_2 \text{ are the frequencies at which } Y = \pm 1 \tag{15a}$$

$$Q_{EXT} = \frac{f_o}{f_3 - f_4} \quad \text{where } f_3, f_4 \text{ are the frequencies at which } Y = \pm (G + 1) \tag{15b}$$

$$Q_o = \frac{f_o}{f_5 - f_6} \quad \text{where } f_5, f_6 \text{ are the frequencies at which } R = \pm X \tag{15c}$$

f_o = resonant frequency which makes Z_{ss} pure real; $(X = 0)$

The function Z_{ss}/Z as a function of frequency is a circle in the complex z plane. A conformal mapping is made to the complex Γ plane where Γ is the complex reflection coefficient defined by:

$$\Gamma = \frac{Z_{ss}/Z - 1}{Z_{ss}/Z + 1}$$

Γ as a function of frequency will also be a circle in the complex Γ plane. As a result of the property of conformal mappings which map circles into circles the complex Γ plane becomes a "Smith Chart" when lines of constant R, X, Y, G are displayed.

The complex Γ circle can be measured and displayed using a polar plot network analyzer. As the frequency is varied about resonance $(X = 0)$, this circle will intersect the lines $R = \pm X$, $Y = \pm 1$, $Y = \pm(G + 1)$. The intersection frequencies thus allow the determination of Q_L, Q_{EXT} and Q_o, using Equations 15a, 15b and 15c. The resonant frequency is determined

from the intersection of the circle with the horizontal axis. Figures 7a and 7b show the above method of measurement and the test set up. The signal from the sweep oscillator is split into two equal signals, a reference and a test. The test signal reflected from the cavity and the reference signal are made to travel equal paths by adjusting the sliding short. The two signals are combined in the harmonic converter, down shifted in frequency and sent to the network analyzer where the phase and amplitude of the test signal are measured and displayed in polar form as shown in Figure 7a.

MEASUREMENT OF MODE STRUCTURE

The longitudinal mode structure in the cavity is determined by moving a small dielectric probe through the cavity and measuring the resonance frequency shift. Since the frequency shift is proportional to the square of the electric field at the position of the dielectric, a plot of the square root of frequency shift versus probe position will reproduce the longitudinal profile of the electric field. Such a measurement is shown in Figure 8 and compares quite favorably with the mode profile of the same cavity determined numerically in Figure 3 of Section I.

G7286

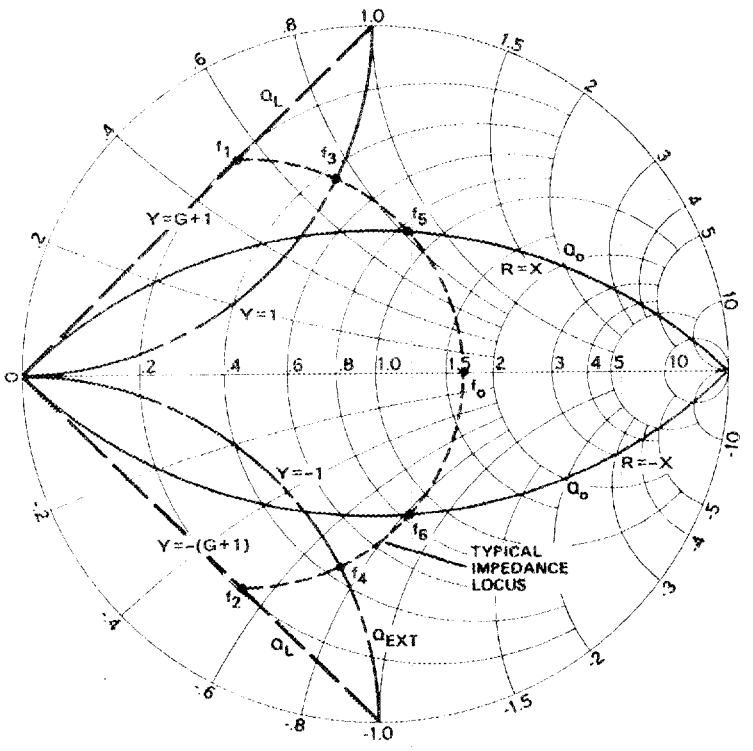

$$Q_{EXT} = f_o/(f_3 - f_4)$$

$$Q_L = f_o/(f_1 - f_2)$$

$$Q_o = f_o/(f_5 - f_6)$$

Figure 7a Smith chart with Loci of Q_o, Q_L, Q_{EXT}.

G7287

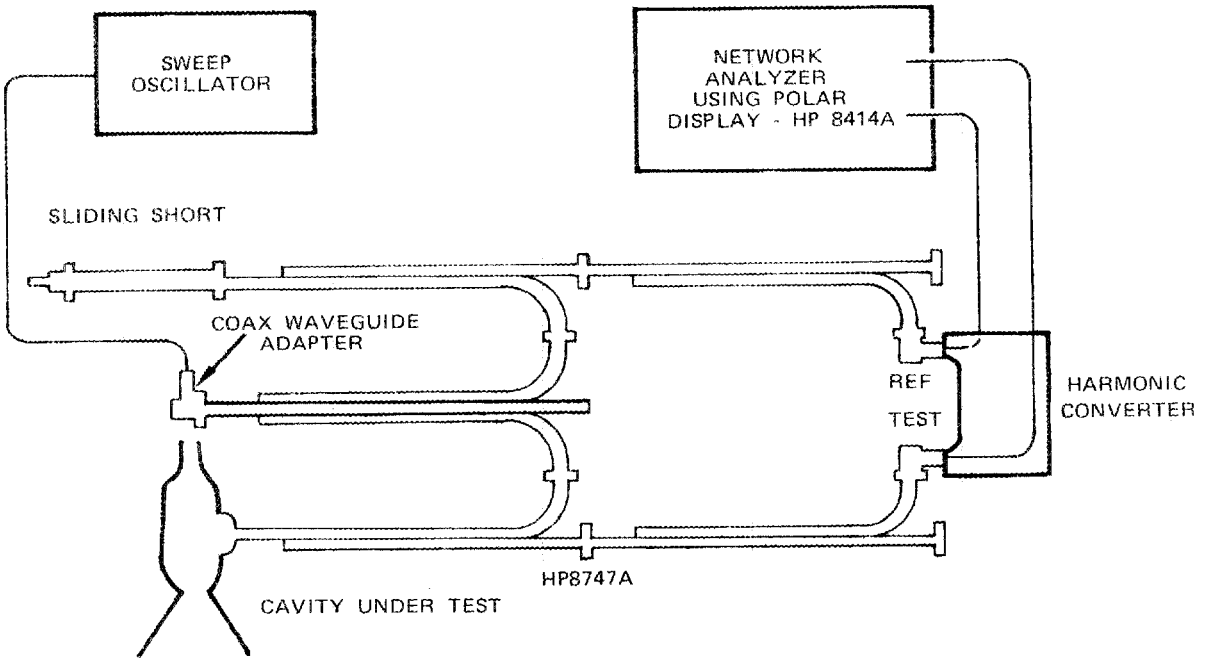

Figure 7b Experimental test set up for Q measurement.

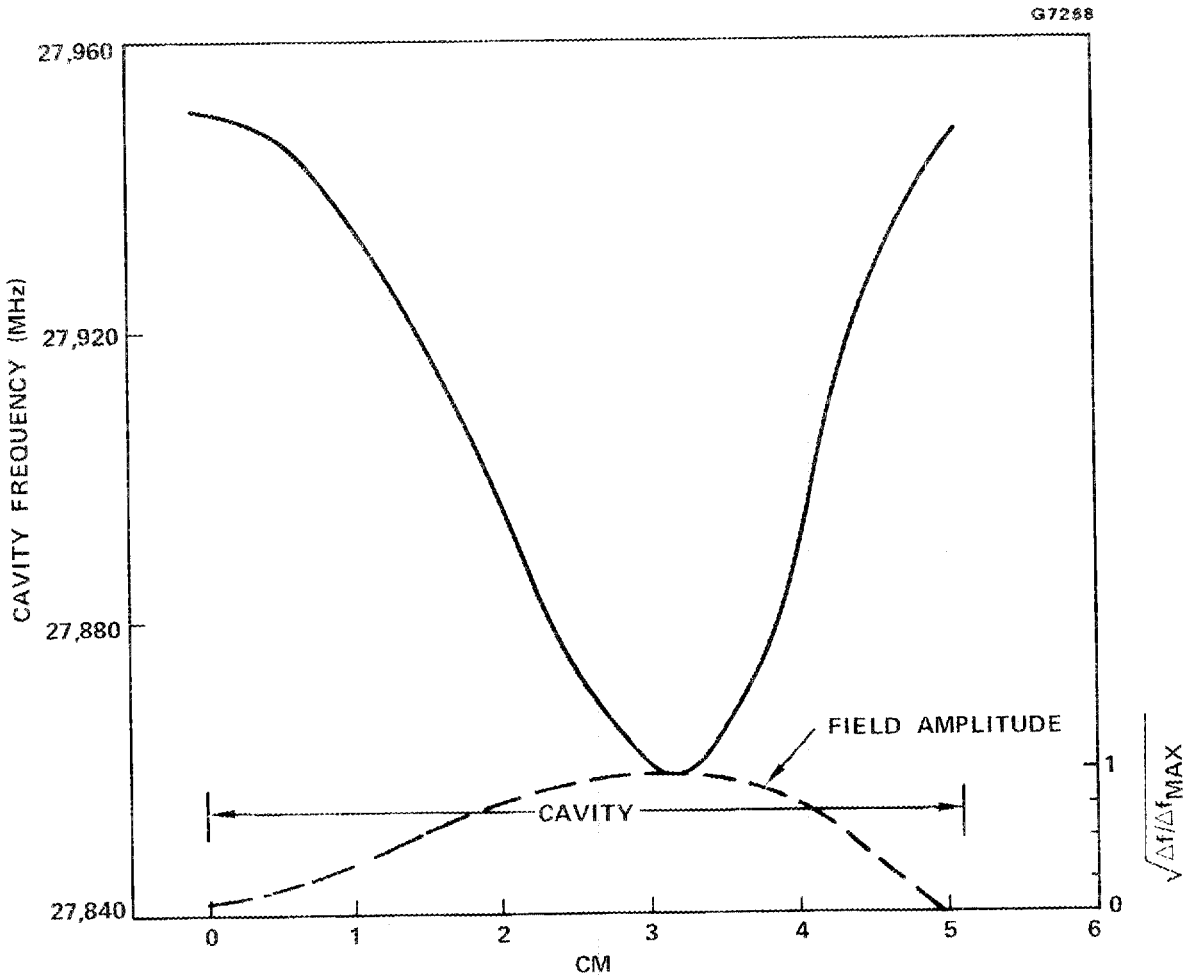

Figure 8 Cavity frequency of TE_{021} mode vs axial position of dielectric probe.

IV. DETERMINATION OF CAVITY OUTPUT POWER AND EFFICIENCY

To calculate the efficiency of a gyrotron oscillator, the self-consistent steady state peak electric field amplitude in the cavity must be found which will require the RF power supplied by the beam to be equal to the RF power drained from the cavity due to the external Q. A large signal program is used to calculate the output power by computing the trajectories of random ensemble of test electrons passing through the RF and DC fields of the cavity calculated in Section I. The trajectories are determined from the relativistic equations of motion given in normalized form by:

$$\frac{dR}{dt} = \frac{U_R}{\gamma} \tag{16a}$$

$$\frac{d\theta}{dt} = \frac{1}{R}\frac{U_\theta}{\gamma} \tag{16b}$$

$$\frac{dz}{dt} = \frac{U_z}{\gamma} \tag{16c}$$

$$\frac{dU_R}{dt} = \frac{U_\theta B_z}{\gamma} + \frac{U_\theta^2}{R\gamma} \tag{16d}$$

$$\frac{dU_\theta}{dt} = E_\theta - \frac{U_R B_z}{\gamma} + \frac{U_z B_R}{\gamma} - \frac{U_\theta U_R}{\gamma R} \tag{16e}$$

$$\frac{dU_z}{dt} = E_z - \frac{U_\theta B_R}{\gamma} \tag{16f}$$

where:

$$E_\theta = \bar{E}_\theta J_1 \left[\frac{k_{mn}R}{a(z)}\right] [E_R(z) \cos \omega t - E_I(z) \sin \omega t] \tag{17a}$$

$$B_R = \frac{\bar{E}_\theta}{\omega/c} \cdot J_1 \left[\frac{k_{mn}R}{a(z)}\right] \left[\frac{dE_R(z)}{dz} \sin \omega t + \frac{dE_I}{dz}(z) \cos \omega t\right] - \frac{B_o(z)R}{2} \tag{17b}$$

$$B_z = -\frac{k_{mn}\bar{E}_\theta}{\omega/c} J_o \left[\frac{k_{mn}R}{a(z)}\right] [E_R(z) \sin \omega t + E_I(z) \cos \omega t] + B_o(z) \tag{17c}$$

$E_R(z)$ and $E_I(z)$ are the axial field profiles obtained numerically from the differential equation of Section I or experimentally, if preferred. $\bar{E}_\theta$ is the peak field in the cavity. $B_o(z)$ is the profile of the external magnetic field and is given by:

$$B_o(z) = \bar{B}_o \left[1+(z-L/2)\cdot \mathrm{DELTB}/L\right] \tag{18}$$

$\bar{B}_o$ is the average magnetic field and DELTB is the percent variation of the magnetic field. The cavity profile is given by a(z).

Solving the above system for up to 1000 test electrons allows one to determine the energy lost by the beam to the RF fields giving the RF power produced. For each value of peak electric field amplitude (Figure 9), the power is optimized with respect to the external magnetic field. One thus generates numerically a function relating the optimum RF power supplied

```
*******************************
*                             *
* DESIGN PARAMETERS ARE       *
*                             *
*******************************

PINPT BEAM INPUT POWER IN KWATTS ...... 6.400D+02
CUROP OPERATING CURRENT IN AMPS ....... 8.000D+00
POUTS OUTPUT POWER IN KWATTS .......... 2.680D+02
VOLTS THE BEAM VOLTAGE ................ 8.000D+04
RCAOP THE RADIUS OF THE CAVITY ........ 1.207D+00
RBMOP THE BEAM GUIDING CENTER RADIUS... 3.139D-01
NCYCL NUMBER OF CYCLOTRON PERIODS...... 1.838D+01
CLENG THE LENGTH OF THE CAVITY......... 5.083D+00
FREQU THE FREQUENCY OF OPERATION....... 2.800E+10
EFFIC THE EFFICIENCY OF INTERACTION.... 4.187D-01
BFILD THE OPERATING FIELD IN GAUSS..... 1.079D+04
ALPHA VELOCITY RATIO BETAP/BETAZ ...... 1.500D+00
GAMAT THE BEAM GAMMA FACTOR ........... 1.157D+00
EAMPL NORMALIZED FIELD AMPLITUDE ...... 3.100D-01
XFACT MAGNETIC MISTUNING FACTOR........ 9.700D-01
PERCENT SPREAD IN VPERP................ 0.0
PERCENT SPREAD IN VZ................... 0.0
PERCENT TAPER IN MAGNETIC FIELD........ 0.0


REQUIRED CAVITY Q ..................... 4.709D+02
REQUIRED LOSS CONSTANT ................ 2.789D+03
ACTUAL CAVITY Q ....................... 4.548D+02
ACTUAL LOSS CONSTANT .................. 2.887D+03
RADIAL MODE NO ........................ 2
AZIMUTHAL MODE NO ..................... 0
EFFECTIVE LMODE ....................... 1.272E+00
CYCLOTRON HARMONIC ....................1
```

Figure 9 Typical computer output from a beam simulation which generates one point on the power supply curve of power output vs field amplitude.

by the beam to the peak electric field amplitude squared $\bar{E}_\theta^2$. For a given fixed current I, this function is symbolically written as:

$$\boxed{P_{supplied} = P_{RF}\ (E_\theta^2, I)} \tag{19}$$

From Section I, the power drained from the cavity through the coupling hole is written as:

$$\boxed{P_{LOSS} = KLOSS\ .\ \bar{E}_\theta^2} \tag{20}$$

with KLOSS being determined by either theoretical or experimental "cold tests".

Since the steady state demands that the power produced $P_{supplied}$ equals the power lost P_{LOSS}, the following equation for the peak electric field amplitude $\bar{E}_\theta^2$ is obtained:

$$\boxed{P_{RF}\ (\bar{E}_\theta^2,\ I) = KLOSS \cdot \bar{E}_\theta^2} \tag{21}$$

The above equation is solved graphically for $\bar{E}_\theta^2$ by determining the intersection of the cavity loss line P_{LOSS} with the power production curve P_{RF}. The solution determines the self-consistent value of $\bar{E}_\theta$, giving the actual output power and efficiency of the cavity.

The cavities described in Section I were analyzed for efficiency. The straight cavity (Figures 2 and 10) showed an efficiency of 32% at 8 amps. The cavity Q was much too high to allow optimum efficiency although

threshold currents were as low as 2 amps. Figure 11 shows the effect of putting a 0.485° taper on the cavity wall (cavity shown in Figure 3). The taper not only allows the basic power production to increase, but it creates a much lower Q_{EXT} which allows the optimum power solution to be realized. In this case, the efficiency was 42%.

Figure 12 shows the solution for the tapered cavity at different currents. No solution exists below 4 amps. Thus, although the tapered cavity has higher efficiency, it requires higher start oscillation currents than a nontapered cavity (4 amps compared to 2 amps). Figure 13 shows a plot of efficiency and external Q as a function of taper angle. One notes the optimum taper at $\sim 0.5^{\circ}$ and the optimum Q_{EXT} at 440.

Instead of tapering the cavity wall, one may slope the magnetic field profile. Figure 14 shows a plot of efficiency versus percent magnetic taper in a straight cavity, assuming that the optimum Q is always possible to achieve in each case. A field taper of 11% would allow an efficiency of 47%. However, it is not obvious that this is attainable since the straight cavity has a Q of 900, much higher than required here ($Q_{EXT} \sim 350$ to realize 47% efficiency). One might try magnetic tapering with cavity tapering in order to bring down the Q and thus realize the high efficiencies. Figure 15 shows the increase in efficiency with magnetic tapering for an actual realizable Q_{EXT} of 559.

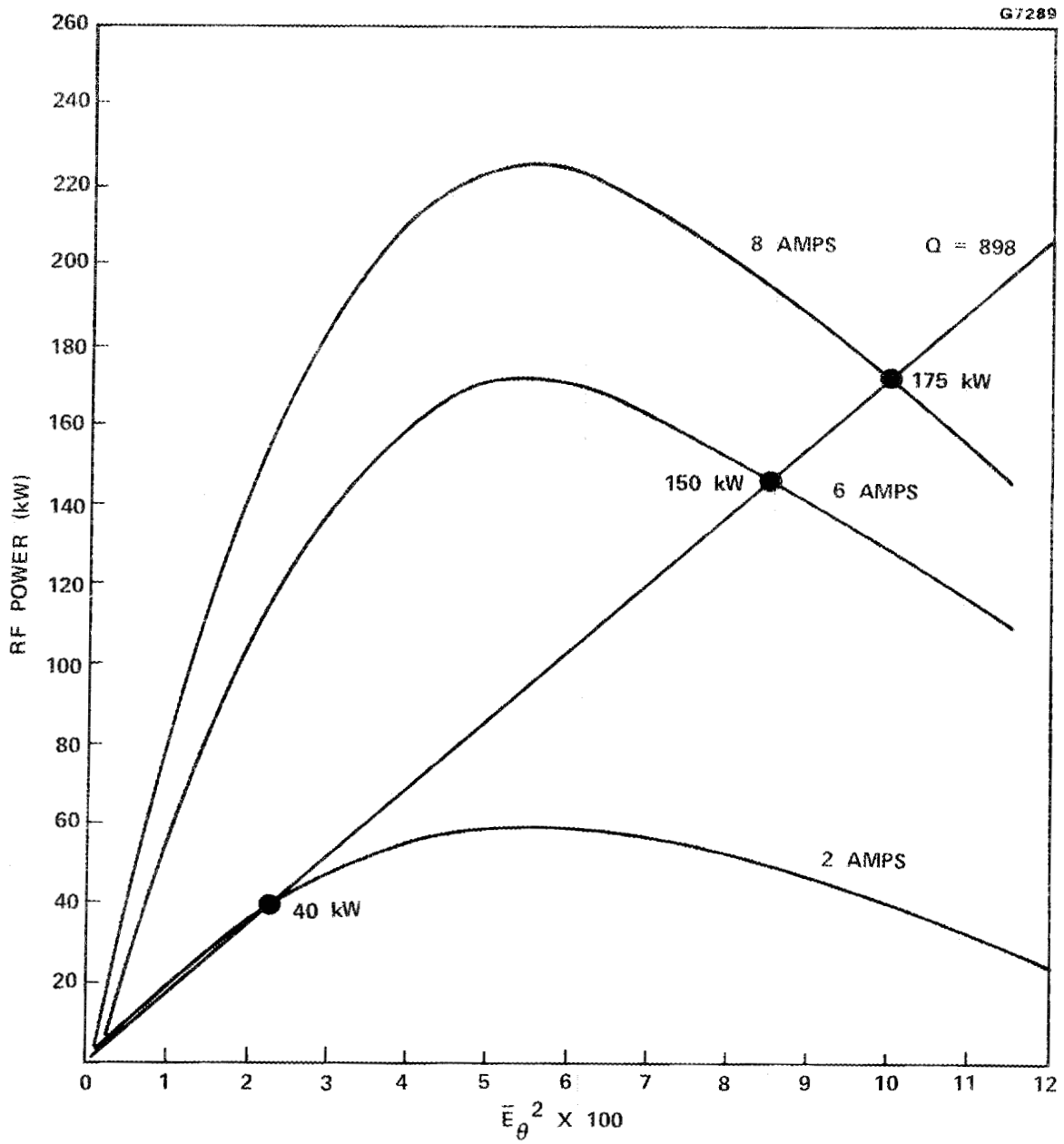

Figure 10 Straight cavity solution of $P_{RF}(\bar{E}_\theta^2, I) = KLOSS\ \bar{E}_\theta^2$.

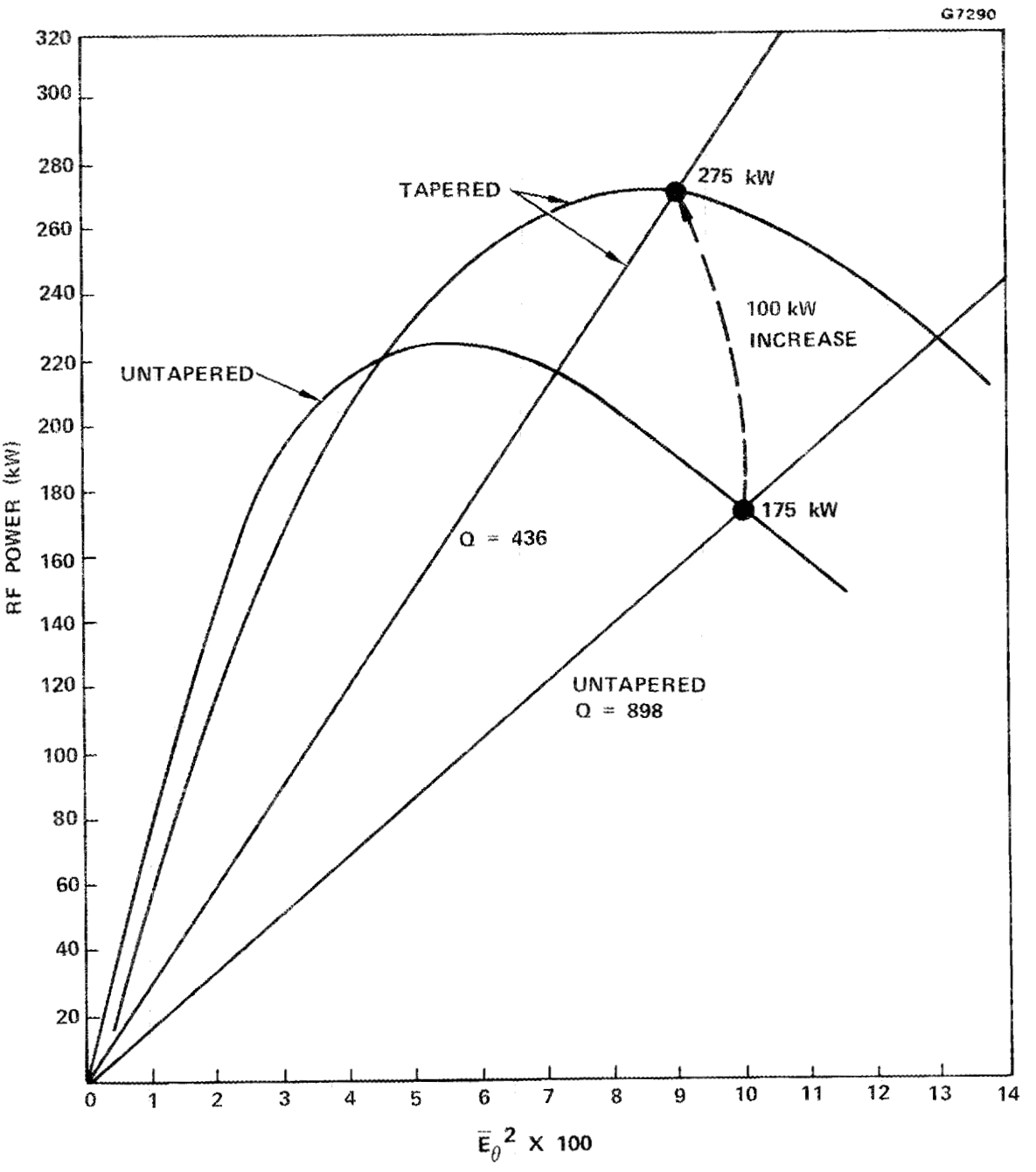

Figure 11 Tapered vs non tapered cavity (0.485° taper).

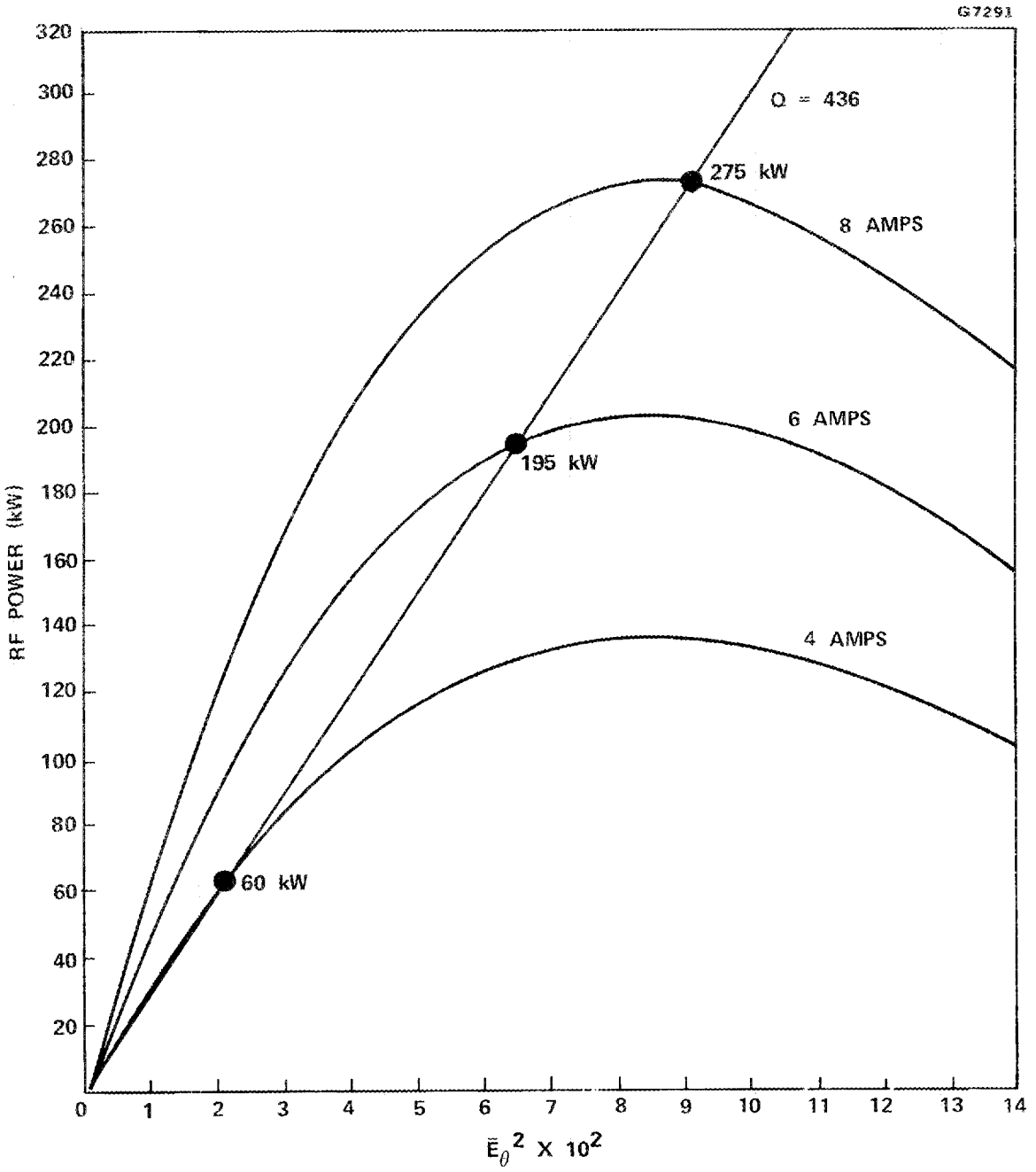

Figure 12 Tapered cavity (0.485°) solution of P_{RF} ($\bar{E}_\theta^2$, I) = KLOSS $\bar{E}_\theta^2$.

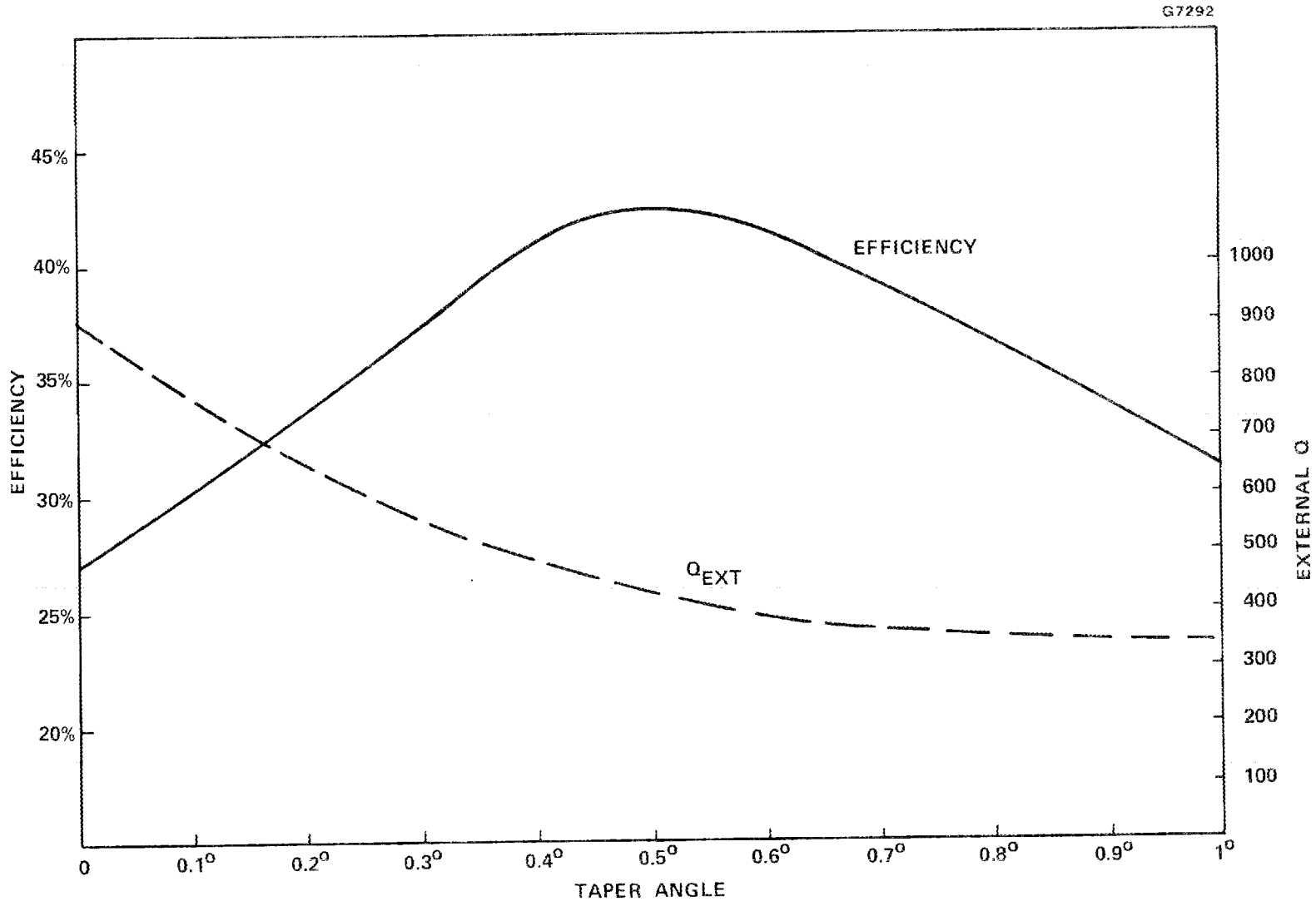

Figure 13 Efficiency and external Q vs taper angle.

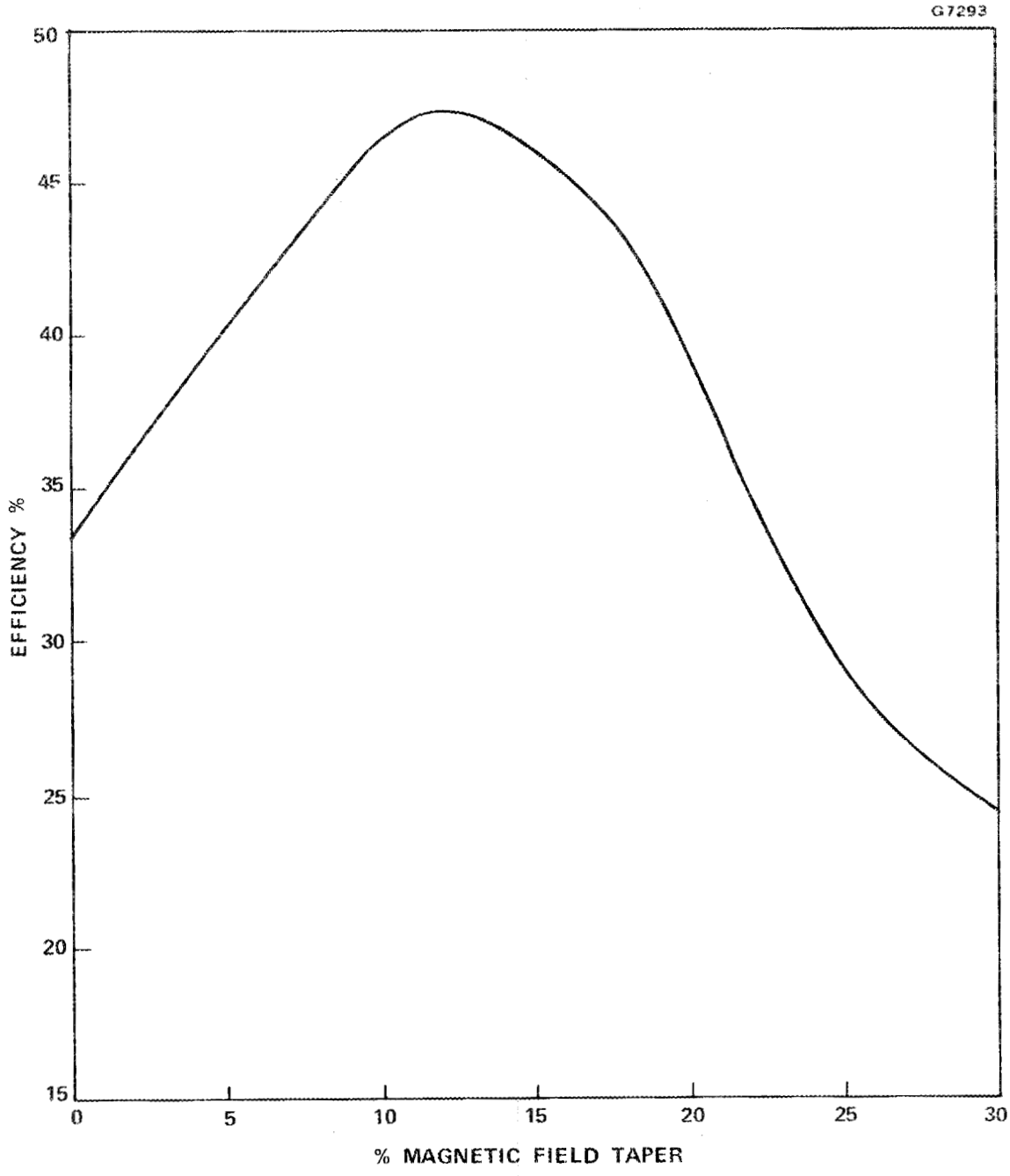

Figure 14 Possible efficiency vs percent taper of magnetic field cavity wall is untapered.

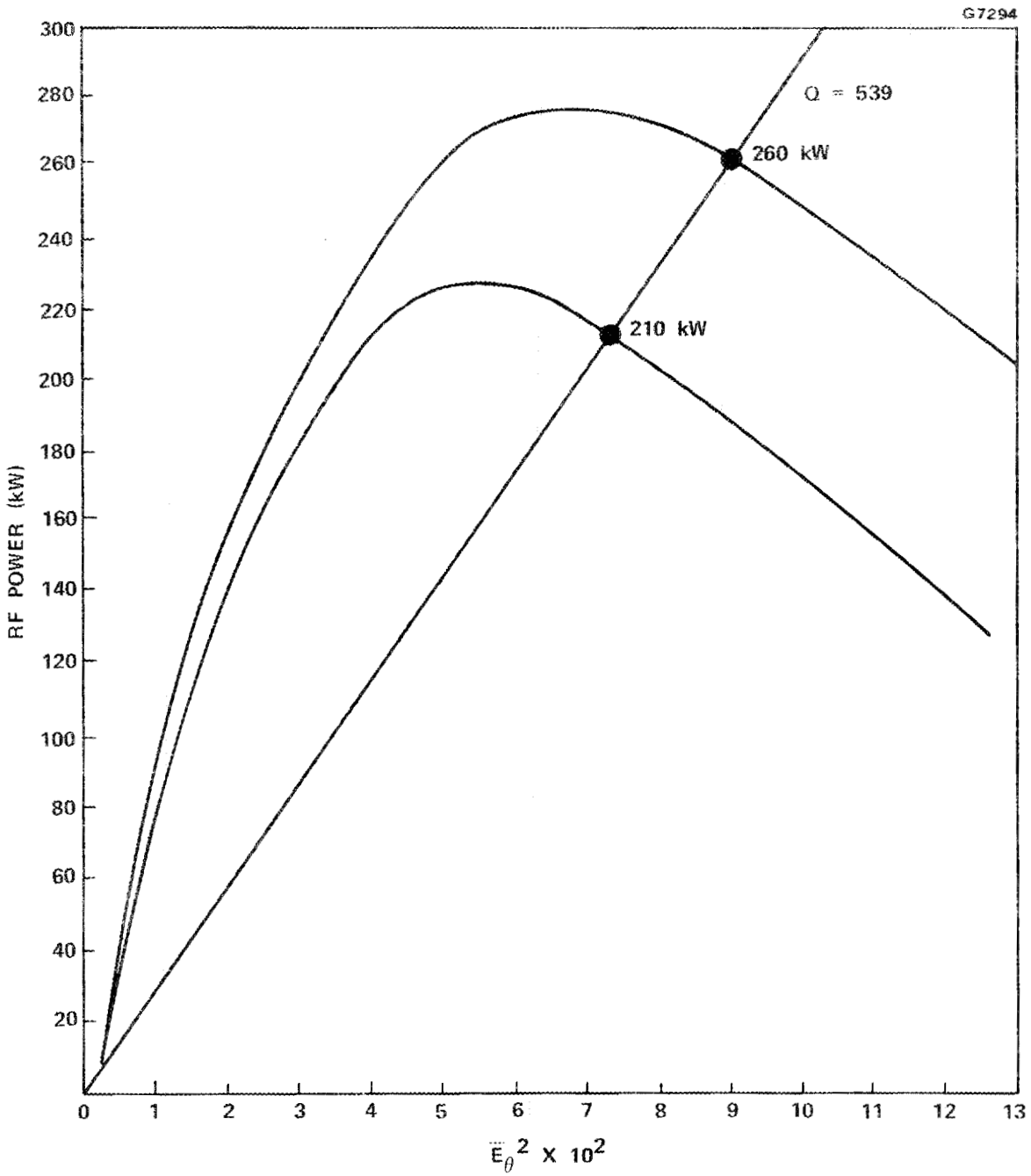

Figure 15 7% magnetic taper vs no magnetic taper.

V. RF POWER DISSIPATION

Assuming operation in the TE_{021} mode at 60 GHz, the wall loss Q is given as:

$$Q_{wall} \simeq \frac{22832 \cdot k_{20}}{\sqrt{60}} \simeq 20{,}000.$$

The power dissipated on the walls is thus given as:

$$\text{power (walls)} = \frac{Q_{EXT}}{20{,}000} \cdot \text{power out.}$$

Using the results of Figure 13, the power dissipated per square centimeter as a function of Q_{EXT} can be calculated and is displayed in Figure 16. To keep wall loading below 1000 watts per square centimeter, it is required to keep Q_{EXT} below 800. External loading which causes reflections could violate this requirement.

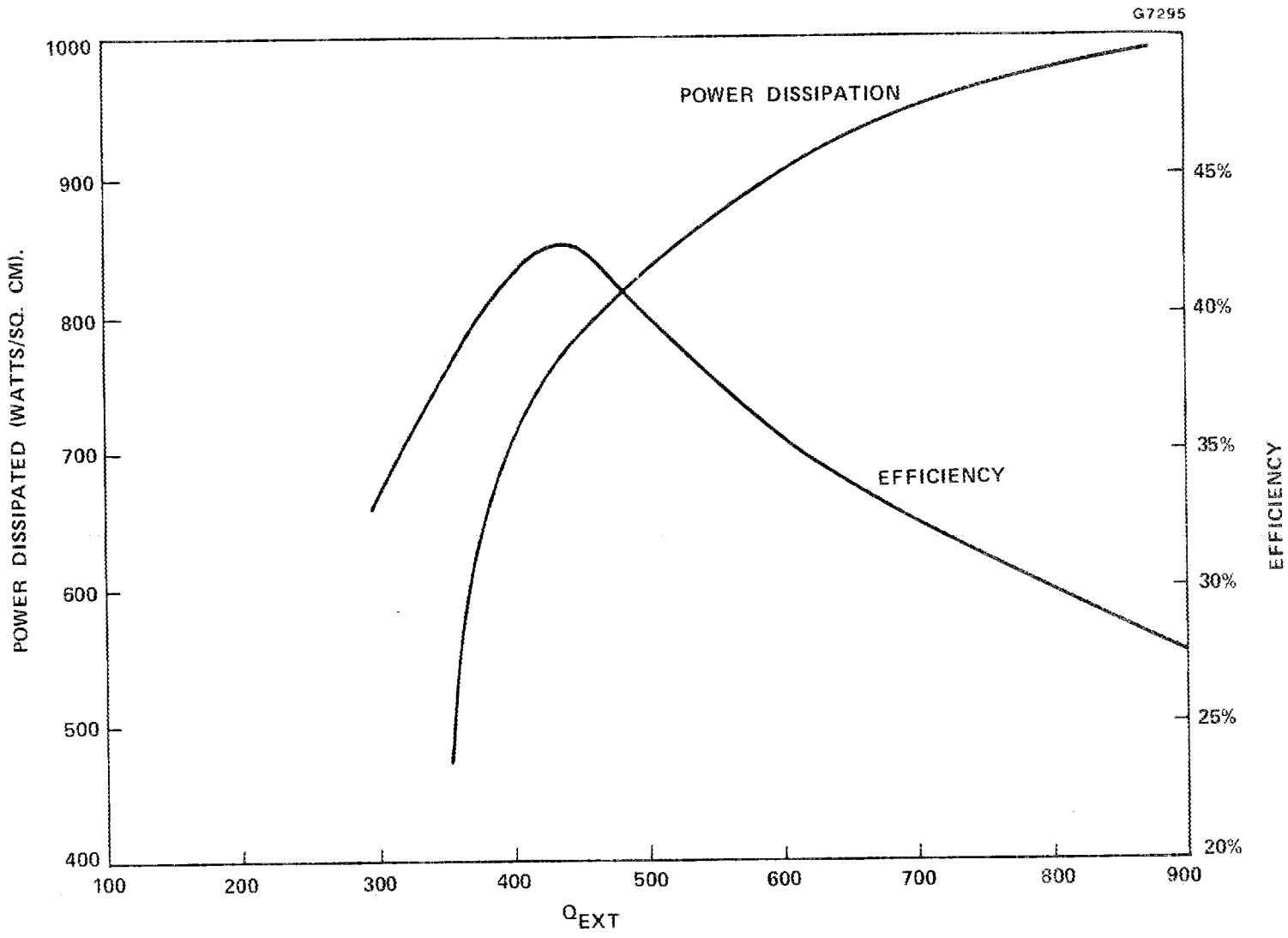

Figure 16 Power dissipation and efficiency vs Q_{EXT}.

VI. CONCLUSIONS AND FUTURE STUDY

It has been shown that cavity tapering and magnetic field tapering can enhance gyrotron efficiency by up to 50%. In both cases the physical mechanism involved is to force the beam to first undergo strong transverse pre bunching. The subsequent RF interaction is then greatly enhanced. Cavity tapering also allows the required Q_{EXT} to be realized. For purposes of having cavity isolation mode stability and low threshold currents, high values of Q_{EXT} are desirable. However for high efficiency and low RF wall dissipation, low Q values are required. Future design work, apart from making improvements in efficiency must find a proper compromise among these conflicting criteria.

REFERENCES

1. S. N. Vlasov et al. "Open Resonators in the Form of Waveguides of Variable Cross Section," Radiofizika Vol. 12, No. 8, 1969 pp 1236 - 1244.

2. E. Ginzton, Microwave Measurements, McGraw-Hill Book Co., Inc., NY, 1957 pp 391, 434.

3. Arnold, K. W., et al, "Development Program for a 200 kw, cw, 110 GHz Gyrotron," Quarterly Report No. 1, June through September 1979, prepared for Oak Ridge National Laboratory, Oakridge, TN 37830, under contract W-7405-ENG-26.

4. Jory et al, "Development Program for 200 kw, cw, 28 GHz Gyroklystron Quarterly Report No. 5. April 1977, prepared for Oak Ridge National Laboratory under Contract 53X01617C.

5. Sprangle, P. and Smith, R. A., "The Non-Linear Theory of Efficiency Enhancement in the Electron Cyclotron Maser," NRL Memorandum Report 3983, April 18, 1979.

ORNL/SUB-33200C
7/24/80

INTERNAL DISTRIBUTION

1. L. A. Berry
2. A. L. Boch
3. J. L. Burke
4. R. J. Colchin
5-8. H. O. Eason
9. O. C. Eldridge
10. R. P. Jernigan
11-12. C. M. Loring
13. H. C. McCurdy
14. O. B. Morgan, Jr.
15. G. F. Pierce
16. T. L. White
17-18. Laboratory Records Department
19. Laboratory Records, ORNL-RC
20. Y-12 Document Reference Section
21-22. Central Research Library
23. Fusion Energy Division Library
24. Fusion Energy Division Communications Center
25. ORNL Patent Office

EXTERNAL DISTRIBUTION

26. R. A. Dandl, 1122 Calle De Los Serranos, San Marcos, CA 92069
27. A. N. Dellis, Culham Laboratory, Abingdon, Oxon, England, OX143DB
28. W. P. Ernst, Princeton University, Plasma Physics Laboratory, P.O. Box 451, Princeton, NJ 08540
29. W. Friz, AFAL/DHM, Wright Patterson AFB, OH 45433
30. T. Godlove, Particle Beam Program, Office of Inertial Fusion, Department of Energy, Mail Stop C-404, Washington, DC 20545
31. V. L. Granatstein, Naval Research Laboratory, Code 6740, Washington, DC 20375
32. G. M. Haas, Component Development Branch, Office of Fusion Energy (ETM), Department of Energy, Mail Stop G-234, Washington, DC 20545
33. J. L. Hirshfield, Yale University, Department of Engineering and Applied Science, P.O. Box 2159, Yale Station, New Haven, CT 06520
34. H. Ikegami, Institute of Plasma Physics, Nagoya University, Nagoya 464, Japan
35. H. Jory, Varian Associates, 611 Hansen Way, Palo Alto, CA 94303
36. J. V. Lebacqz, Stanford Linear Accelerator Center, P.O. Box 4349, Stanford, CA 94305
37. W. Lindquist, Electronics Engineering Department, Lawrence Livermore Laboratory, P.O. Box 808/L-443, Livermore, CA 94550
38. K. G. Moses, TRW Defense & Space Systems, 1 Space Park, Bldg. R-1, Redondo Beach, CA 90278
39. M. R. Murphy, Office of Fusion Energy (ETM, Department of Energy, Mail Stop G-234, Washington, DC 20545
40. V. B. Napper, Three Dunwoody Park, Suite 112, Atlanta, GA 30341
41. B. H. Quon, TRW Defense & Space Systems, 1 Space Park, Bldg. R-1, Redondo Beach, CA 90278
42. M. E. Read, Naval Research Laboratory, Code 6740, Washington, DC 20375
43. D. B. Remsen, General Atomic Company, P.O. Box 81608, San Diego, CA 92138
44. B. Stallard, Lawrence Livermore Laboratory, University of California, L-437, P.O. Box 808, Livermore, CA 94550
45. H. S. Staten, Office of Fusion Energy (ETM), Department of Energy, Mail Stop G-234, Washington, DC 20545
46. P. Tallerico, AT-1, Accelerator Technology Division, Los Alamos Scientific Laboratory, Mail Stop 817, P.O. Box 1663, Los Alamos, NM 87545

INDEX
4 11/16 PHOTOMASTER (DOUBLE 4 1/16 x 11 5/8 COLUMN)
UCTION (FINISH SIZE 8 1/2 X 11 - DOUBLE 3 1/16 X 8 11/16 COLUMN)

EXTERNAL DISTRIBUTION (continued)

47. R. J. Temkin, National Magnet Laboratory, Massachusetts Institute of Technology, Cambridge, MA 02139
48. A. Trivelpiece, Science Applications, Inc., 1200 Prospect Street, P.O. Box 2351, LaJolla, CA 92038
49. Director, U.S. Army Ballistic Missle Defense Advance Technology Center, Attn.: D. Schenk, ATC-R, P.O. Box 1500, Huntsville, AL 35807

50-51. Department of Energy Technical Information Center, Oak Ridge, TN 37830

52. RADC/OCTP, Griffiss AFB, NY 13441
53. Office of Assistant Manager for Energy Research and Development, Oak Ridge Operations Office, Department of Energy, Oak Ridge, TN 37830

EX
1/15 PHOTOMASTER (DOUBLE 4 1/16 X 11 5/8 COLUMN)
TION (FINISH SIZE 9 1/2 X 11 - DOUBLE 3 1/16 X 9 11/16 COLUMN)